Glycobiology vol. 11 no. 12 pp. 1051–1070, 2001

Modeling human congenital disorder of glycosylation type IIa in the mouse: conservation of asparagine-linked glycan-dependent functions in mammalian physiology and insights into disease pathogenesis

Yan Wang[2], Jenny Tan[3], Mark Sutton-Smith[4], David Ditto[5], Maria Panico[4], Robert M. Campbell[2], Nissi M. Varki[6], Jeffrey M. Long[2,7,8], Jaak Jaeken[9], Simon R. Levinson[10], Anthony Wynshaw-Boris[2,7,8], Howard R. Morris[4], Dzung Le[5], Anne Dell[4], Harry Schachter[3], and Jamey D. Marth[1,2]

[2]Department of Cellular and Molecular Medicine, Howard Hughes Medical Institute, Glycobiology Research and Training Center, 9500 Gilman Drive-0625, University of California San Diego, La Jolla, CA 92093, USA; [3]Program in Structural Biology and Biochemistry, Hospital for Sick Children, and Department of Biochemistry, University of Toronto, Toronto, Ontario, Canada; [4]Department of Biochemistry, Imperial College of Science, Technology and Medicine, London, England; [5]Department of Pathology, University of California San Diego, La Jolla, CA 92093, USA; [6]Department of Medicine, Glycobiology Research and Training Center, University of California San Diego, La Jolla, CA 92093, USA; [7]Department of Pediatrics, University of California San Diego, La Jolla, CA 92093, USA; [8]Superfund Basic Research Center, University of California San Diego, La Jolla, CA, 92093 USA; [9]Department of Paediatrics, Centre for Metabolic Disease, University of Leuven, Leuven, Belgium; [10]Department of Cellular and Structural Biology, University of Colorado Health Sciences Center, Denver, CO, USA

Received on July 24, 2001; revised on August 30, 2001; accepted on August 31, 2001

The congenital disorders of glycosylation (CDGs) are recent additions to the repertoire of inherited human genetic diseases. Frequency of CDGs is unknown since most cases are believed to be misdiagnosed or unrecognized. With few patients identified and heterogeneity in disease signs noted, studies of animal models may provide increased understanding of pathogenic mechanisms. However, features of mammalian glycan biosynthesis and species-specific variations in glycan repertoires have cast doubt on whether animal models of human genetic defects in protein glycosylation will reproduce pathogenic events and disease signs. We have introduced a mutation into the mouse germline that recapitulates the glycan biosynthetic defect responsible for human CDG type IIa (CDG-IIa). Mice lacking the *Mgat2* gene were deficient in GlcNAcT-II glycosyltransferase activity and complex N-glycans, resulting in severe gastrointestinal, hematologic, and osteogenic abnormalities. With use of a lectin-based diagnostic screen for CDG-IIa, we found that all *Mgat2*-null mice died in early postnatal development. However, crossing the *Mgat2* mutation into a distinct genetic background resulted in a low frequency of survivors. Mice deficient in complex N-glycans exhibited most CDG-IIa disease signs; however, some signs were unique to the aged mouse or are prognostic in human CDG-IIa. Unexpectedly, analyses of N-glycan structures in *Mgat2*-null mice revealed a novel oligosaccharide branch on the "bisecting" N-acetylglucosamine. These genetic, biochemical, and physiologic studies indicate conserved functions for N-glycan branches produced in the Golgi apparatus among two mammalian species and suggest possible therapeutic approaches to GlcNAcT-II deficiency. Our findings indicate that human genetic disease due to aberrant protein glycosylation can be modeled in the mouse to gain insights into N-glycan-dependent physiology and the pathogenesis of CDG-IIa.

Key words: CDG-IIa/disease/genetics/glycosylation/N-glycans

Introduction

Abnormalities in carbohydrate (glycan) production have been increasingly recognized as causes of human genetic disease. In the early 1990s, a test normally used to detect alcohol consumption revealed the first of the childhood syndromes now called the congenital disorders of glycosylation (CDGs) (reviewed in Jaeken *et al.*, 1991, 2001). Hundreds of children are known to be affected, but the extent of CDG in the human population is unknown at this time because testing is sporadic and relies on a diagnostic technique involving serum transferrin isoelectric focusing (Westphal *et al.*, 2000). CDG type I (CDG-I) syndromes reflect mutations in different enzymes responsible for construction of the dolichol pyrophosphate oligosaccharide precursor, resulting in reduced levels and altered structures of the precursor (reviewed in Jaeken and Carchon, 2000). This leads to a reduced efficiency of protein N-glycosylation, which can be detrimental to protein stability and maturation in the endoplasmic reticulum (reviewed in Ellgaard *et al.*, 1999; Parodi, 2000).

A second class of CDG (type II) has also been identified by aberrant serum transferrin mobility wherein the defect is in the processing and diversification of protein-bound N-glycan structure, and not the efficiency of N-glycosylation site usage or transit through the secretory pathway (Jaeken *et al.*, 1994). CDG type IIa (CDG-IIa) is due to an autosomal recessive lesion in the human *MGAT2* gene, residing on chromosome 14 at q21, which encodes UDP-GlcNAc:α-6-D-mannoside β-1,2-*N*-acetylglucosaminyltransferase II (GlcNAcT-II, E.C.2.4.1.143), a Golgi-bound glycosyltransferase essential for the production of complex-type N-glycans present in the Golgi, on cell surfaces, and among extracellular compartments (Charuk *et al.*, 1995; Tan *et al.*, 1996; Schachter and Jaeken, 1999). Only four

[1]To whom correspondence should be addressed

patients have been described at this writing, and the oldest is now 20 years of age. In two of those cases the diagnosis was made after the age of 8 years (Jaeken *et al.*, 1994; Engelhardt *et al.*, 1999; Cormier-Daire *et al.*, 2000).

CDG-IIa indications include a general failure to thrive, dysmorphic facial features, feeding difficulties, and psychomotor retardation. Patients are incapable of speech and undergo occasional epileptic seizures. Also observed are osteopenia, kyphoscoliosis, blood coagulopathies, immune defects, gastrointestinal abnormalities, ventricular septal defect of the heart, and susceptibility to infection. Studies of cells from patients with CDG-IIa reveal deficiency in complex N-glycans and a predominance of hybrid-type structures that include terminal mannose linkages. Four mutations in the human *MGAT2* gene have been described thus far, all of which reside in the catalytic domain of GlcNAcT-II (Ser290Phe; His262Arg; Asn318Asp; Cys339Ter). Mutations analyzed *in vitro* by recombinant approaches thus far have shown that each abolishes enzyme activity and may decrease protein stability (Tan *et al.*, 1996).

Inherited genetic alterations in carbohydrate synthesis exist among mammalian species and many glycan structures differ between mice and humans. Examples include the ABO blood group antigens (Koda *et al.*, 2000), the α1-3Gal xenotransplantation antigen (Galili and Swanson, 1991), and the dominance of N-acetyl sialic acid in humans due to the null mutation in the N-glycolylneuraminic acid synthase gene (Chou *et al.*, 1998). Such genetic events cause widespread alterations of terminal saccharide linkages that are present on various glycan branches. These alterations may have substantial consequences since terminal saccharide linkages can be essential in defining the physiologic functions of glycan branches. Expression of glycan branches and terminal structures can be altered in normal and aberrant physiology by transcriptional mechanisms acting on glycosyltransferase gene promoter sequences. Moreover, glycosyltransferase expression patterns and not substrate specificity per se can be a key factor in determining physiologic function. For example, an inherited genetic mutation in the glycosyltransferase gene *Galgt2* alters cell lineage expression and in this manner creates a novel function involving the homeostasis of von Willebrand factor in circulation (Mohlke *et al.*, 1999).

Most glycosyltransferases, including GlcNAcT-II, exhibit a high degree of specificity for glycan substrates from data obtained in *in vitro* enzymatic studies, and therefore may not be influenced by glycoprotein amino acid sequence contexts. Moreover, because some glycosyltransferases can compete for the same glycan substrates, the outcome involving modification of a glycoprotein in the milieu of various glycosyltransferases is at present difficult to predict (Schachter, 1991). Glycans further provide essential components of pathogen receptors in hosts, and glycosyltransferase alterations during phylogeny may reflect an evolutionary "arms race" ascribed to such pathogen–host interactions (Gagneux and Varki, 1999). For example, the expression of α2-6 sialic acid linkages on red blood cells and epithelium differs between mice and humans; this difference can influence the tissue and species tropism of viral infections, such as influenza (Carroll *et al.*, 1981; Suzuki *et al.*, 2000).

These features of glycan expression and biosynthesis render uncertain the degree to which glycosyltransferases are subject to the axiom that evolutionary conservation of gene sequences and biochemical activity reflects conservation of physiologic function. Comparing two mammalian species with the same genetic deficiency in the N-glycan repertoire would provide an assessment of the degree of conservation of N-glycan function and may lead to increased understanding of N-glycan structure–function relationships. In addition, studies recapitulating a genetic lesion causing CDGs may provide insights into the pathogenesis of human CDG syndromes.

We have therefore generated a complex N-glycan deficiency by inactivating the mouse *Mgat2* gene, and compared phenotypes with human CDG-IIa patients. Our findings reveal that there is significant conservation of complex-type N-glycan branch function between these two species with aberrant gastrointestinal, osteogenic, and hematologic processes that promote disease. In the course of our studies, we have also developed a simpler, more accurate biochemical diagnostic test for CDG-IIa. Unexpectedly, we have discovered the presence of genetic modifiers of disease signs in the mouse genome and a novel N-glycan branch structure induced by the absence of the *Mgat2* gene. These results also suggest that most human CDG-IIa cases may be undiagnosed or misdiagnosed and may represent a cause of early human infant lethality.

Results

Mgat2 gene expression, mutagenesis and role in postnatal viability

The *Mgat2* gene exists with a single protein-encoding exon and is conserved as a single copy homologue among mammals analyzed, including mice and humans. All cells studied from both species produce complex N-glycans, although levels of *Mgat2* RNA can differ significantly among tissues (Figure 1A). Genomic DNA encoding the mouse *Mgat2* gene was isolated and used to construct a targeting vector that incorporated Cre-loxP recombination for conditional mutagenesis (Figure 1B). Embryonic stem cells generated with the desired alterations at the targeted *Mgat2* locus were confirmed by genomic Southern blotting (Figure 1C). The conditional mutation (F) was transmitted through the germ line and mice heterozygous for the loxP-flanked *Mgat2* allele (F) were bred with ZP3-Cre transgenic mates to produce the deleted (Δ) allele, by methods previously described (Shafi *et al.*, 2000). Heterozygous offspring were identified, appeared overtly normal, and were fertile (Figure 1D and data not shown). Mutant mice were analyzed during breeding into the C57BL/6 strain background for up to five generations, and mice homozygous for the loxP-flanked *Mgat2* allele (F/F) were unaffected. Embryos homozygous for the $Mgat2^{\Delta}$ allele and postembryonic day (E) 9 were found *in utero* at frequencies slightly lower than expected, due to an increase in embryonic lethality between E9 and E15 (not shown). However, more than 75% survived, yet by embryonic day (E) 15 these embryos were smaller, approximately 80% the size of littermates retaining a functional *Mgat2* gene (not shown). Other than their smaller size, there were no observed pathologic indications of disease or developmental defects. However, newborn mice homozygous for the $Mgat2^{\Delta}$ allele were often ignored or cannibalized by the mothers, and others failed to feed. Only 1% survived into the second week of

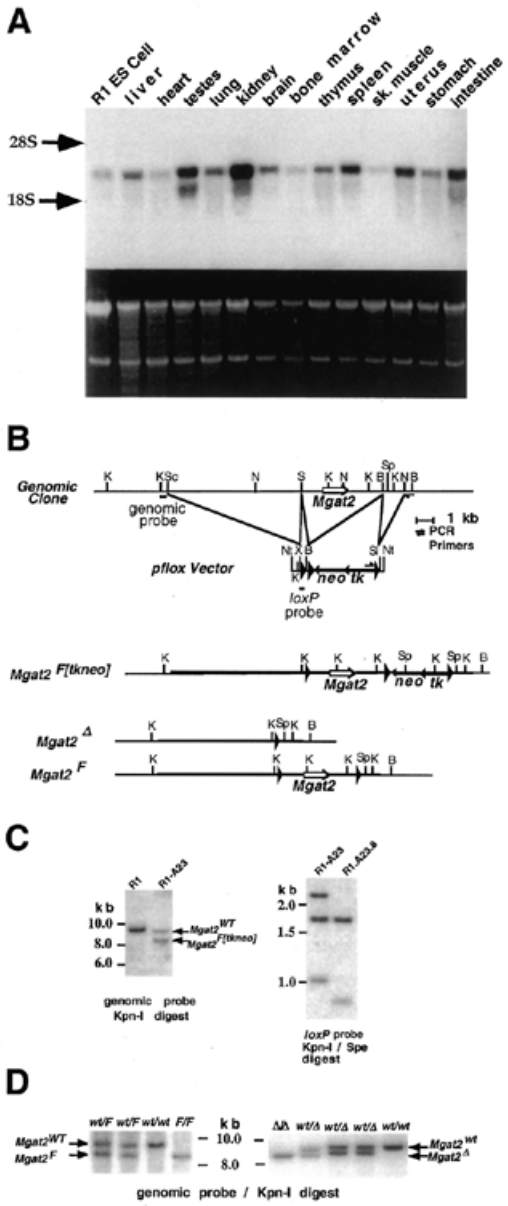

Fig. 1. Expression, structure, and deletion of the mouse *Mgat2* gene using Cre-loxP recombination. (**A**) *Mgat2* gene is widely expressed in tissues, but at different levels. Total RNA was hybridized with a mouse *Mgat2* genomic probe, revealing a single band of approximately 3.0 kb. The bottom panel shows the ethidium bromide–stained profile indicating intact and relatively similar RNA levels in each sample. (**B**) A mouse genomic clone of the *Mgat*2 gene and the pflo*x* vector containing *tk* and *neo* markers were used to produce the systemic ($Mgat2^{\Delta}$) and conditional ($Mgat2^{F}$) mutations. (**C**) DNA from targeted ES clone R1-A23 harbored the 8.6 kb (F[tkneo]) allele and the parental (R1) 9.6-kb wild-type (wt) allele (left panel). Using clone R1-A23, Cre-loxP recombination and ganciclovir selection resulted in the ES subclone R1-A23.8 bearing the $Mgat2^{F}$ allele (right panel). Clone R1-A23.8 was used to produce chimeric mice to transmit the mutation into the germline. (**D**) Southern analysis of tail DNA from chimeric and heterozygote matings confirmed presence of the $Mgat2^{F}$ allele (left panel). Crossing mice bearing the $Mgat2^{F}$ allele to ZP3-Cre transgenic mice (Shafi *et al.*, 2000) resulted in germ line recombination yielding the $Mgat2^{\Delta}$ allele (right panel). Southern blot analyses are from tail DNA. Restriction enzyme sites: K, Kpn-I; Sc, Sac I; N, Nco-I; B, BamH-I; Sp, Spe-I; Sl, Sal-I; X, Xba-I.

postnatal life, and even with nurturing none lived longer than 4 weeks.

Dependence of complex N-glycan biosynthesis on Mgat2-encoded GlcNAcT-II

GlcNAcT-II activity was analyzed in various tissues prior to 4 weeks of age, and the activities reflected approximately the tissue expression profile of *Mgat2* RNA. Mice heterozygous for the $Mgat2^{\Delta}$ allele generally contained less GlcNAcT-II activity, although in some cell types normal levels remained. In contrast, GlcNAcT-II activity was insignificant among tissues of mice bearing the Δ/Δ genotype (Figure 2A). We did, however, observe a low level in the intestine of such mice; however, the molecular source of this activity is unknown at present. All tissues continued to produce *Mgat1*-encoded GlcNAcT-I activity, a more proximal step in N-glycan biosynthesis necessary for the formation of hybrid-type N-glycans (Figure 2A). A decrease in GlcNAcT-I activity seemed to occur among a few tissues of *Mgat2*-null mice. Nevertheless, significant levels of GlcNAcT-I remained. These results confirm that the *Mgat2* gene is necessary for encoding GlcNAcT-II activity among various tissues *in vivo*.

We compared human and mouse serum transferrin isoelectric focusing patterns, as carried out in the clinical diagnostic assay for CDG-IIa. In the absence of *Mgat2*, mouse transferrin undergoes mobility alterations similar to those observed in human CDG-IIa reflecting fewer N-glycan branches and thereby fewer terminal sialic acid residues (Wada *et al.*, 1992; Yamashita *et al.*, 1993; Figure 2B). However, a simple, rapid and accurate assay that distinguishes between the many CDG-I variants and CDG type IIa might be more useful in diagnostic approaches. In this regard we found that E-PHA lectin reactivity can be employed as a diagnostic screen for mouse and human *Mgat2* deficiency. Analyses of small amounts of whole blood from human CDG-IIa patients and from *Mgat2*-null mice, either by immobilization on nitrocellulose or by flow cytometry, revealed that phytohemagglutinin (PHA) binding is absent from the mutant samples (Figure 2C and data not shown). Flow cytometric approaches are especially capable of providing quantitative measurements of lectin binding, which may be useful in possible cases of partial GlcNAcT-II deficiency.

We further assessed N-glycan structures by histochemistry using the plant lectin L-PHA (Figure 2D). Organs and tissues from *Mgat2*-deficient mice appeared normal; however these tissues did not bind L-PHA lectin, whereas wild-type tissues did, indicating a deficiency in GlcNAcT-V N-glycan branch formation. This is consistent with the loss of complex N-glycans as GlcNAcT-II activity is essential for GlcNAcT-V substrate formation. Some remaining L-PHA binding was present in the intestine, a tissue that also retained a low level of GlcNAcT-II activity. These findings indicate that *Mgat2* is required for complex N-glycan biosynthesis *in vivo*, but do not establish the exact structures that remain. Biophysical analyses of N-glycan structures by mass spectrometric methods were undertaken to confirm these findings and to provide insights into N-glycan biosynthesis *in vivo* in the absence of *Mgat2* function (see *Results*).

Dysmorphic features and severe locomotor retardation

Those *Mgat2*-null mice surviving to at least 8 days of age were approximately half the size of littermates that retained a functional

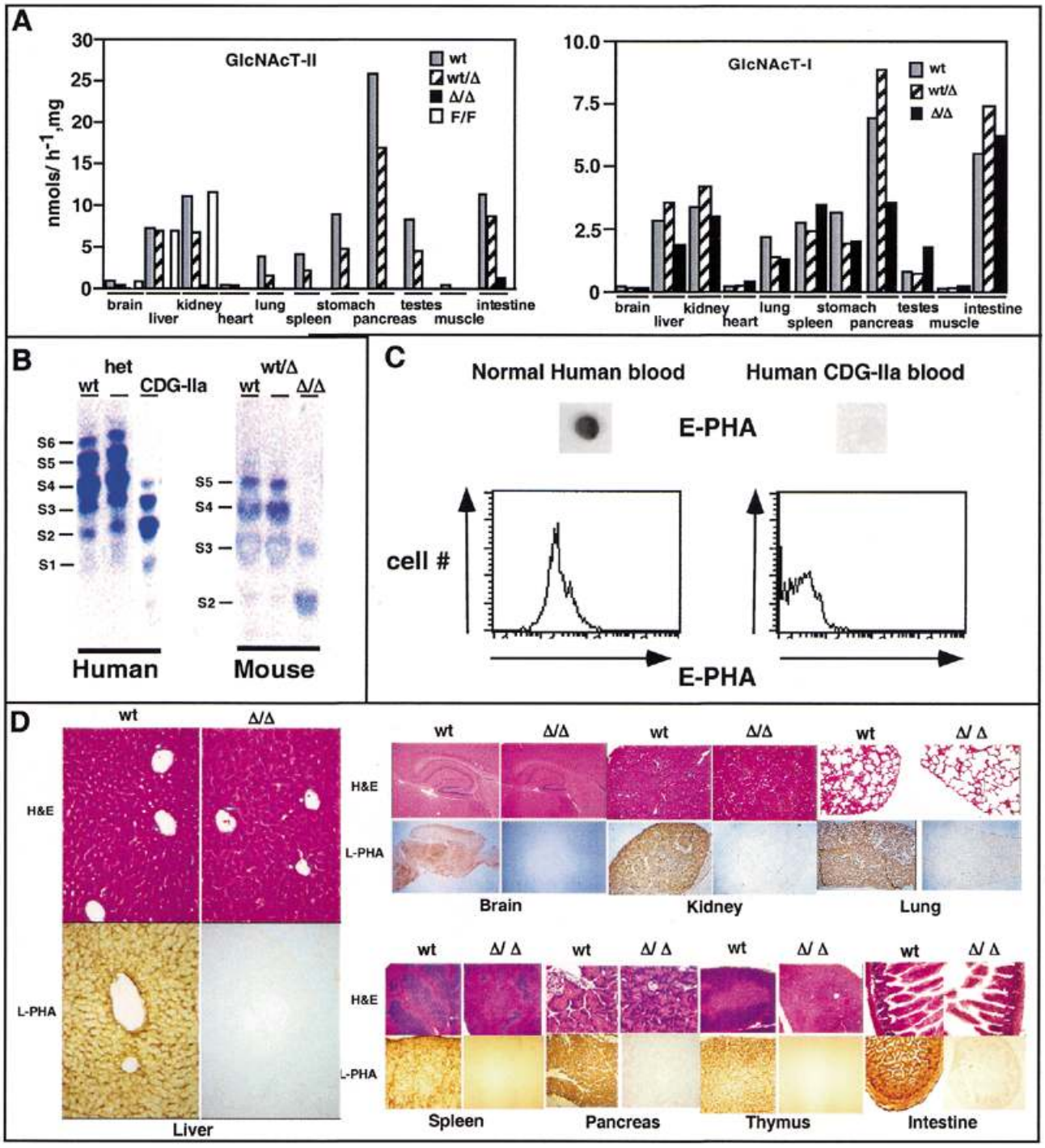

Fig. 2. GlcNAcT-I and GlcNAcT-II activities and *N*-glycan biosynthesis in the absence of *Mgat2*. (**A**) The mutation in the *Mgat2* gene resulted in the loss of GlcNAcT-II activity except for some residue activity in intestine. GlcNAcT-I activity remained normal in most tissues but was reduced in some *Mgat2*-null samples for unknown reasons ($N = 2$ for all samples). (**B**) Isoelectric focusing of serum transferrin from normal and CDG-IIa human blood, and from normal and *Mgat2* mutant mouse blood. S1 to S6: number of sialyl residues per molecule of transferrin. (**C**) E-PHA binding to normal or CDG-IIa whole blood was visualized after blotting 5 µl to nitrocellulose or in solution by flow cytometry (see *Materials and methods*). Identical results were obtained using L-PHA (not shown). (**D**) L-PHA staining and hematoxylin/eosin staining on various tissues. Wild-type tissues bound L-PHA strongly, whereas homozygous *Mgat2* mutant tissues failed to bind L-PHA. Magnifications on hematoxylin/eosin-stained sections are: 25× (brain); 50× (spleen, thymus); 100× (kidney); 200× (liver, lung, intestine); and 400× (pancreas). Magnifications on L-PHA stained sections are 50× except brain (5×), intestine (100×), and liver (200×).

Mgat2 allele. They exhibited dysmorphic facial features and severe locomotor deficits. Reduced muscular development was apparent, as was a hunched spinal column, indicating scoliosis (Figure 3A). Transient paralysis and tremors similar to

epileptic seizures were observed in approximately 20% of *Mgat2*-null mice. Further histologic examinations revealed that the brain developed normally and the various anatomical subregions, including the cortex, hippocampus, olfactory bulb, and brainstem structures, were unremarkable. Additionally, the cerebellum was of proportional size and contained a normal complement of viable Purkinje cells (data not shown).

Neuromuscular synaptic transmission in the absence of Mgat2

The characteristics of neuromuscular transmission in the diaphragms of *Mgat2* nulls were compared with wild-type and with heterozygous littermates (Figure 3B). Significantly larger miniature endplate potentials (minis) and evoked endplate responses were seen in the absence of *Mgat2* than in either wild-type or heterozygous neuromuscular synapses, and the quantal content of the evoked responses was slightly but significantly reduced at *Mgat2*-null synapses. All other characteristics tested (e.g., kinetics, mini frequency) failed to demonstrate significant differences between diaphragms from nulls and littermates retaining a functional *Mgat2* gene. In no cases were significant differences observed between wild-type and heterozygous preparations.

Thus synaptic transmission appeared to be enhanced in *Mgat2*-nulls versus either wild-type or heterozygous littermates. Although this was initially unexpected given the motor deficits characteristic of many of the *Mgat2*-null animals, we believe the explanation to be a straightforward effect of reduced muscle fiber diameter resulting from the retarded growth of null animals. As with most other anatomical structures, *Mgat2*-null muscle fibers were of smaller dimensions when viewed microscopically (not shown). This readily accounts for the increased amplitudes of minis and evoked responses observed, as it has been previously demonstrated that the increased longitudinal internal resistance of smaller-diameter muscle fibers in early pre- and postnatal development results in larger mini and evoked synaptic potentials recorded at the endplate (Katz and Thesleff, 1957). In addition, the reduced quantal content of evoked responses in *Mgat2*-nulls may be related to smaller endplate areas expected in these muscle fibers, such as occur in early development (Bennett and Florin, 1974). Similar explanations have been given for changes in neuromuscular transmission seen in diaphragm and other skeletal muscles of growth-retarded athymic nude mice (Schofield and Marshall, 1980).

Osteopenia with increased osteoclast activity

A significant defect in bone formation was noted in *Mgat2*-null mice. An observed twisting of the hunched spinal column indicated kyphoscoliosis. The entire skeletal system was affected and bones that did develop were poorly calcified and brittle, including the vertebrae, ribs, femur, hips, and skull (Figure 4A). Bone density was quantitatively determined by autoradiographic methods and was found reduced by over 30% among *Mgat2*-null mice (Figure 4B). Joints were also poorly articulated, and fractures were noted in some cases. The formation of secondary ossification sites was delayed such that they were absent at embryonic day 13 in the *Mgat2*-null mice (Figure 4C). Additionally, osteoclast-derived tartrate acid resistant phosphatase activity (TRAP) was found elevated in the femurs (Figure 4D). Normal osteoblast activity was observed (not shown), together suggesting that the net deficiency of bone density is due to increased resorption by osteoclasts.

Hematopoiesis, serum chemistry, and blood coagulopathy

Serum biochemical analyses of *Mgat2*-null mice revealed a decrease in blood glucose, total serum protein and Ca^{2+} levels (Figure 5A). A significant increase in aspartate aminotransferase (AST) was noted without concurrent increase in alanine aminotransferase (ALT), findings that usually rule out infectious hepatitis or inflammatory conditions affecting the liver parenchyma. Increased AST alone may reflect damaged cardiac muscles, damaged skeletal muscles, dermatomyositis, crush muscle injuries, acute pancreatitis, pulmonary embolism, or hemolytic disease. Creatine phosphokinase levels, which are increased in human CDG-IIa, were too variable in the number of mice analyzed to confirm significant changes (not shown). Reduced levels of glucose, protein, and calcium as noted may reflect poor nutritional uptake.

Blood was collected and analyzed using a clinical hemogram analyzer with software modifications suitable for studies of the mouse (Figure 5B). A mild to moderate anemia was present in the *Mgat2*-null mouse, identified by a lower hematocrit value with a 25%–30% reduction in circulating red blood cells. Mean corpuscular volume was increased, and hemoglobin content was reduced consistent with an increase in circulating reticulocytes. These findings are similar to the dyserythropoietic phenotype described in mice lacking alpha-mannosidase-II, an enzyme operating immediately proximal to GlcNAcT-II in the pathway of N-glycan synthesis (Chui *et al.*, 1997). In contrast, platelets were reduced by approximately 50% in the absence of *Mgat2*; however, this degree of platelet reduction in the mouse does not by itself alter blood coagulation (unpublished data).

Factors that regulate blood coagulation are altered among human CDG-IIa patients and may predispose them to thrombosis. In *Mgat2*-null mice, we observed decreases in most procoagulant (clotting) factors and anticoagulant factors protein C and antithrombin, suggesting a defect in liver protein synthesis or release mechanisms (Figure 5C). However, the increased fibrinogen and plasminogen levels and the normal alkaline phosphatase and ALT activities are not consistent with severe liver dysfunction. Markedly decreased levels of protein C and antithrombin relative to the mild decreases in procoagulant factors may predispose these animals to thromboembolic diseases. Furthermore, the increased level of plasminogen with simultaneous decreased levels of its natural inhibitor, alpha-2-antiplasmin, may lead to bleeding as the result of excessive fibrinolysis. Both human and mouse mutants have increased activated partial prothromboplastin time (13%–15% increase). No change in factor VIII or von Willebrand factor was observed (data not shown). Human patients also show a reduction in protein S (60% normal) and factor IX (60% normal); however, levels of these two factors were unaltered in the mouse.

Gastrointestinal abnormalities with deficient mucus production and thrombosis

On necropsy, more than half of *Mgat2*-deficient mice exhibited a distended stomach filled with unprocessed food or gas, suggesting an intestinal obstruction in the region of the pylorus (Figure 6A and data not shown). Obstipation was indicated as constipation was noted, and prolapse of the rectum with

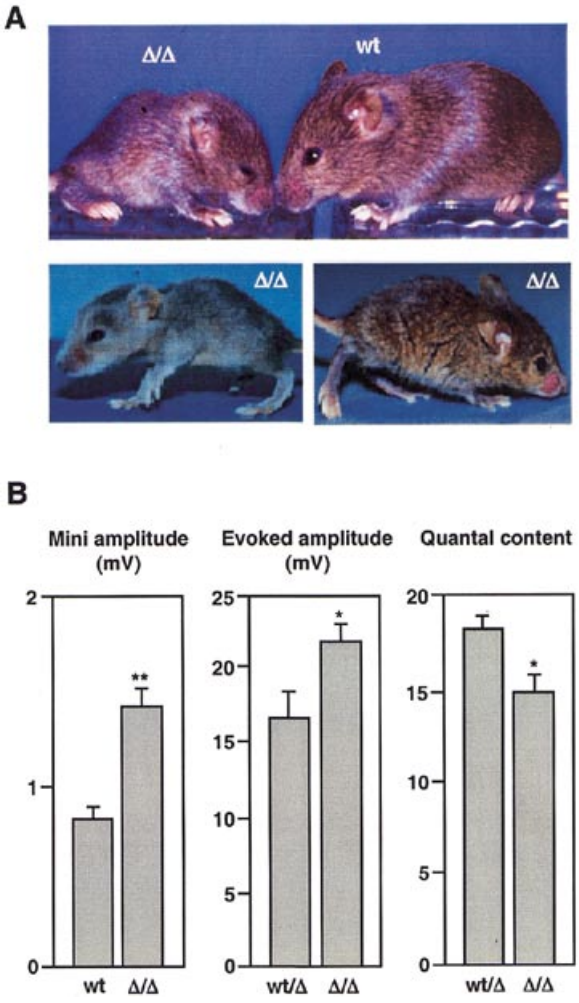

Fig. 3. Dysmorphic features and locomotor defects with analyses of neuromuscular synaptic transmission. (**A**) Representative mutant pups at 2 weeks (upper panel) and 3 weeks (lower panel). Null pups show signs of dysmorphic facial features, scoliosis, and locomotor defects. (**B**) Comparison of neuromuscular transmission properties. Wild-type (wt) and heterozygote (wt/Δ) characteristics were statistically compared with those of the *Mgat2*-nulls (Δ/Δ). *, $p < 0.05$; **, $p < 0.01$ (wt and wt/Δ mini amplitudes were not significantly different).

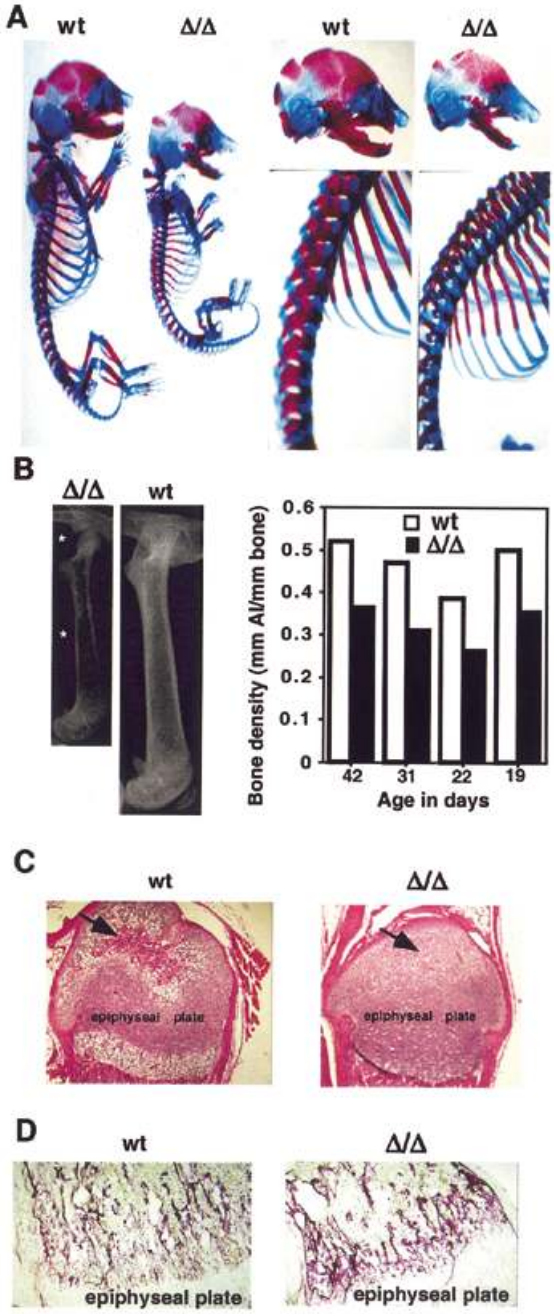

Fig. 4. Osteopenia occurs with retarded bone development and increased osteoclast activity. (**A**) The decreased mineralization in mutants was noted with Alizarin red, which stains bone, and Alcian blue, which stains cartilage. (**B**) Autoradiograph of femur (left panel) demonstrates the reduced bone density on the mice lacking *Mgat2* gene. Joint abnormalities and microfractures are noted (upper asterisk). The optical density per millimeter of the bone (mm Al/mm bone) using aluminum wedge as a reference indicated ~30% reduction in the mutants (right panel). Bone density was determined across a transverse line on the femur at the location of the lower asterisk. (**C**) The secondary ossification center (arrow, left) was absent (delayed) in *Mgat2* mutants (arrow, right) assessed at embryonic day 13. The micrograph illustrates hematoxylin/eosin staining of the head of the mouse femur. Magnification: wt, 50×; Δ/Δ, 100×. (**D**) TRAP staining on cryosections of femur from 1-month-old mice (100×) indicated elevation of osteoclast-derived TRAP activity in the metaphysis near the epiphyseal plate in *Mgat2*-null littermates.

bleeding occurred in several cases. Blood was also found in the lumen of the stomach and intestines in several cases (Figure 6B). Histologic examination revealed normal mucosal epithelial cells; however, a reduction in mucin levels within the mucosal Brunner's glands was evident (Figure 6C). Moreover, similar histochemical studies of the pyloric glands also revealed a significant decrease in mucin levels (Figure 6D). A deficiency in mucin levels within the gastrointestinal tract can result in reduced food motility and digestion, which could lead to constipation and obstipation. We also cannot rule out that ischemic intestines may have resulted from thrombosis of the mesenteric vessels with subsequent bleeding into the intestines. Hemorrhage from submicroscopic mucosal damage not detected on histologic examination may have been contributed and exacerbated by the observed blood coagulopathy.

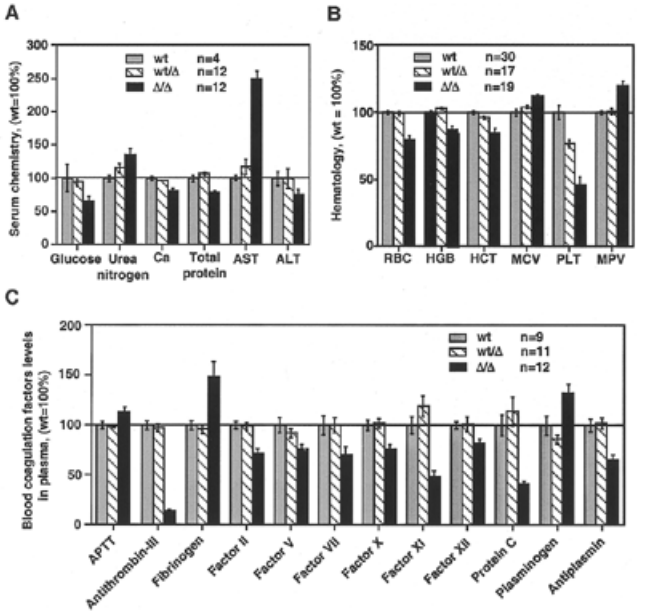

Fig. 5. Blood chemistry (**A**), hematology (**B**), and blood coagulation factor analyses (**C**). Values are presented as % relative to wild-type mice. RBC: red blood cell; HGB: hemoglobin; HCT: hematocrit; MCV: mean corpuscular volume; PLT: platelet count; MPV: mean platelet volume; Ca: calcium; AST: aspartate aminotransferase; ALT: alanine aminotransferase. APTT; activated partial thromboplastin time.

Genetic influence on CDG-IIa severity in Mgat2-deficient mice

An inherited absence of *Mgat2* gene function in the mouse led to lethality by 4 weeks of age; however, no cases of human lethality due to CDG-IIa have been reported. We considered the possibility that genetic modifiers of *Mgat2* function may exist in the genome. During breeding the *Mgat2* mutation through the mouse germ line into the C57BL/6 background, genomic contribution was initially derived by the 129 strain and, increasingly, the C57BL/6 strain. No survivors older than 4 weeks were produced in more than 1000 offspring analyzed during five generations of backcrossing into the C57BL/6 strain.

We next crossed *Mgat2* heterozygotes into the "outbred" ICR strain and monitored the offspring produced between generations three to five. The frequency of *Mgat2*-null mice surviving the first week of life did not change; however, the majority of those that did survive the first week lived beyond 4 weeks of age (Figure 7A). In fact those that survived the first week of life almost always survived for many months but remained smaller than littermates that retained a functional *Mgat2* gene (Figure 7B). These *Mgat2*-null survivors exhibited similar disease signs as described above; however, disease was more variable among individuals and the severity was reduced (Figure 7C and data not shown).

Physical characteristics of 3–9-month-old *Mgat2*-null survivors included thinning fur and a noticeable head tilt with the tendency to circle in the cage. Excessive barbering was observed with loss of facial fur. Locomotor dysfunction was evident and gait abnormalities were demonstrated by paw print analysis (Figure 7D). None of the *Mgat2*-null mice could swim sufficiently for testing in the Morris water maze. Poor ambulatory

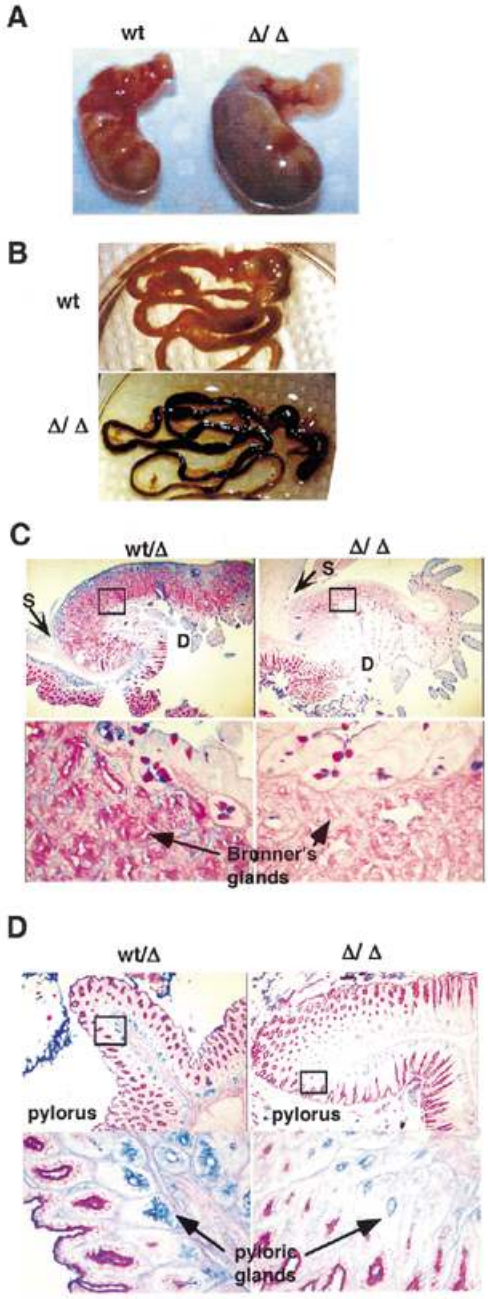

Fig. 6. Gastrointestinal dysfunction with reduced mucin levels, Brunner's gland defects, and hemorrhage. (**A**) Comparison of the stomach from the wild-type and *Mgat2*-null littermate shows that the stomach from the mutant is dilated, in this case with blood. (**B**) A photograph showing a comparison of the intestines from the wild-type and null animals shows that the intestinal tract from the null mouse is filled with blood. (**C**) The upper two panels are low-magnification photomicrographs of the region of the pyloric sphincter and the duodenum from a heterozygous and a *Mgat2*-null littermate. The boxed areas are magnified in the lower panels to demonstrate the submucosal Brunner's glands of the duodenum stained with PAS/Alcian blue pH 2.5. Staining shows lower levels of mucins in the Brunner's glands of the null mouse. Upper panels, 50×; lower panels, 400×. (**D**) The pylorus of the stomach from the heterozygote and the null animals stained with PAS/Alcian Blue pH 2.5 (upper panels, 50×). The boxed areas in the upper panels are magnified in the lower panels (400×) and show that mucin (blue) is present in the crypts at the base of epithelial glands in the heterozygote, whereas only a few crypts in the null animal contain mucins. PAS/Alcian blue at pH 2.5 demonstrates sialomucins and hyaluronic acids as a blue stain and polysaccharides and neutral mucosubstances with a magenta to red stain.

ability included greatly diminished times in the Rotarod test in comparison to heterozygous littermates (Figure 7E). Nociception however appeared normal (data not shown). Muscular function was significantly diminished in analyses of the amount of time that mutant mice were able to support their body weight and by an 80% reduction in grip strength (Figure 7F).

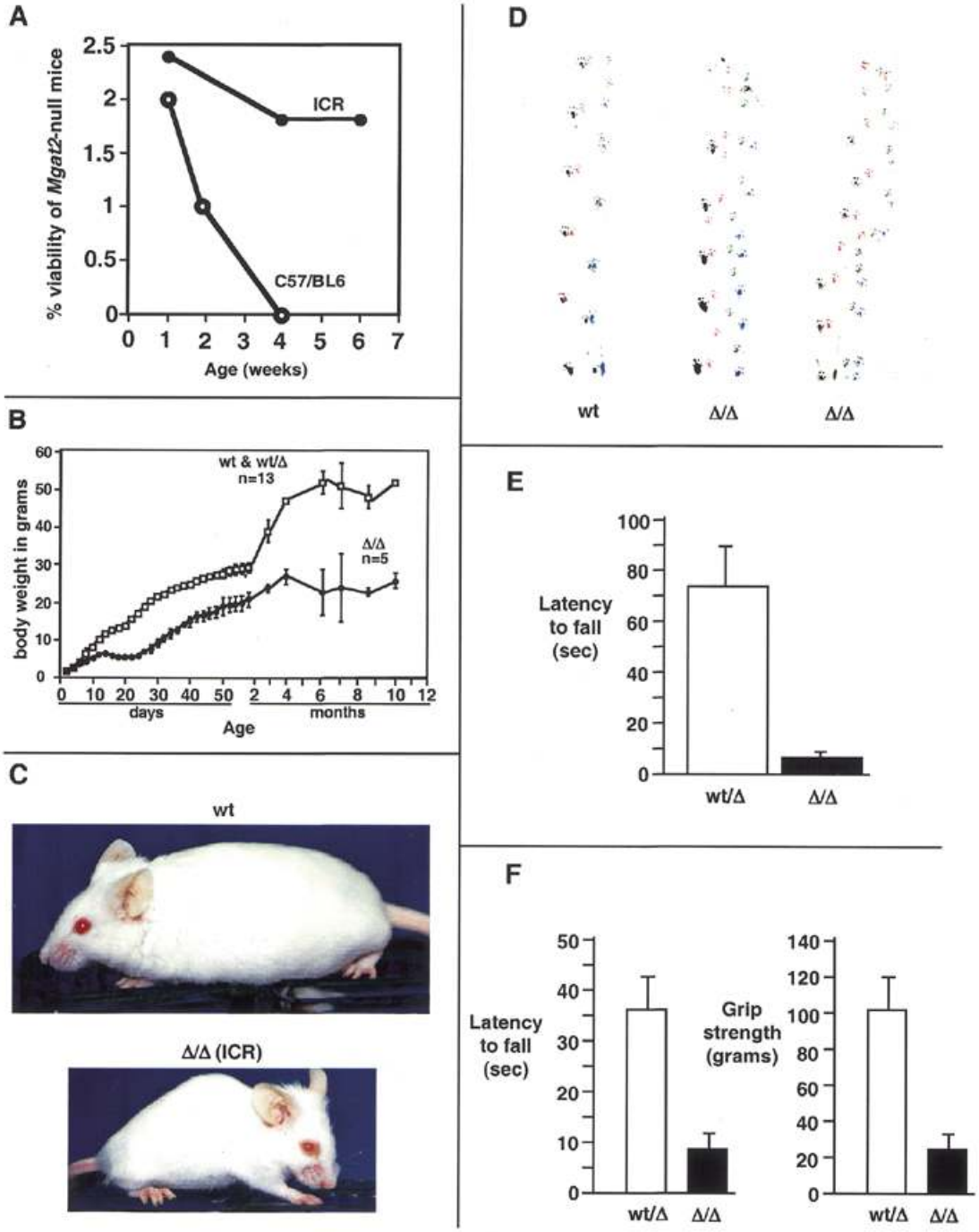

Fig. 7. The genetic background alters disease penetrance and survival of *Mgat2*-null mice. (**A**) None of the *Mgat2*-null mice produced among more than 1000 offspring generated from 160 litters in the 129 and C57BL/6 backgrounds survived past 4 weeks of age. However, survival past 4 weeks of age occurred when the *Mgat2* mutation was bred into the ICR background. The ICR data is derived from 164 pups and 24 litters produced after three to five generations on the outbred ICR-strain. (**B**) The ICR-bred *Mgat2*-null mice are runted in comparison to wild-type or heterozygous littermates at virtually all developmental stages. (**C**) Photograph of *Mgat2*-null mouse and wild-type littermate at the age of 3 months (weight: wt, 38 g; Δ/Δ, 24 g). (**D**) Locomotor dysfunction represented by pawprint pattern analyses of heterozygous and *Mgat2*-null ICR-bred littermates. The null mice move with shorter strides and an uneven pattern compared to the heterozygotes. (**E**) Rotarod performance of the *Mgat2*-null mice was impaired in comparison to heterozygotes [$T(5) = 6.91$, $p < 0.0001$]. (**F**) Two separate tests of strength are presented. Compared to heterozygous littermates, nulls were impaired in both the wire hang test [$T(5) = 4.29$, $p < 0.007$] and in grip strength [$T(5) = 6.82$, $p < 0.001$].

Low fecundity and spermatogenic failure in Mgat2-null survivors

Approximately 30% of female mice lacking the *Mgat2* gene produced offspring; however, they failed to nurture their pups, and the pups died within a few days unless foster mothers were provided. In contrast, male *Mgat2*-null mice exhibited testicular atrophy and were invariably infertile (Figure 8A and data not shown). Spermatogenesis was disrupted and no mature sperm were found in the lumen of the seminiferous tubules (Figure 8B; top panel). Spermatogonia were present, as were spermatocytes; however, a deficiency in spermatids was observed (Figure 8B; middle and bottom panels). The absence of spermatids was confirmed by histochemical analysis with Periodic acid Schiff (PAS) reagent that binds to the acrosomal structures found on developing and mature spermatids (Figure 8C; Russell *et al.*, 1990). The observed loss of early spermatids suggests that GlcNAcT-II activity is essential for the differentiation of spermatocytes into early spermatids. Heterozygous males were unaffected with normal sperm development and abundance (not shown). Moreover, heterozygotes produced normal frequencies of functional sperm bearing the $Mgat2^{\Delta}$ haplotype as judged by genotyping their offspring resulting from breeding with normal wild-type females.

N-glycan analyses of tissues from Mgat2-null mice reveal the loss of complex N-glycans and the presence of a novel branch structure in the kidney

With the use of recently developed mass spectrometry approaches for determining endogenous carbohydrate structures in mammalian tissue (Sutton-Smith *et al.*, 2000; Chui *et al.*, 2001), we screened brain, liver, and kidney for alterations in N-glycans. Fast atom bombardment mass spectrometry (FAB-MS) and gas chromatography mass spectrometry (GC-MS) screening experiments on brain, liver and kidney from *Mgat2*-null mice were fully consistent with the absence of complex-type N-glycan structures bearing branches on the 6-arm of the trimannosyl core. Normal liver has abundant biantennary N-glycan branches (nonbisected) carrying sialylated termini, whereas the most abundant N-glycan in the *Mgat2*-null sample is a sialylated monoantennary species, as expected (not shown). The normal brain is rich in bisected biantennary N-glycans carrying Lewis^x and truncated branches (Sutton-Smith *et al.*, 2000), while the major signals in the absence of *Mgat2* are consistent with monoantennary bisected hybrid-type N-glycan branches, also as expected (not shown). The null kidney also contains predominantly hybrid N-glycans but with signals suggesting the possibility of structures not previously reported. Data acquired from the intestine revealed significant variations that will require extensive future analyses to determine the structural repertoire of N-glycans in this tissue.

Partial FAB mass spectra from permethylated N-glycans released from control and *Mgat2*-null kidney are shown in Figure 9A and 9B, respectively. These data indicate that, as expected, the family of core fucosylated bi-, tri- and tetra-antennary/branched bisected complex N-glycans that occur in high abundance in the normal mouse kidney (Figure 9A; Chui *et al.*, 2001) are absent in the *Mgat2*-null tissue. Instead the *Mgat2*-null sample is characterized by a major new family of N-glycans dominated by a structure of composition $Fuc_3Hex_5HexNAc_4$ (*m/z* 2593) that corresponds to a core fucosylated glycan with two Lewis^x antennae. Other signals present in the mutant but not the normal kidney have compositions corresponding to additional or fewer Fuc and/or Hex residues (*m/z* 2215, 2245, 2419, 2593, 3216). Interestingly, the majority of complex-type N-glycans observed in the wild-type kidney are bisected (Figure 9A), whereas the composition $Fuc_3Hex_5HexNAc_4$ is not consistent with the presence of an unsubstituted bisecting GlcNAc in addition to two Lewis^x branches.

The branch assignments in the *Mgat2*-null spectrum were supported by the presence of major fragment ions at *m/z* 638 (A-type ion of composition FucHexHexNAc), *m/z* 450 (β-cleavage of fucose from *m/z* 638), and *m/z* 432 (elimination of fucose from the *m/z* 638 ion indicating that the fucose is attached at the 3-position of the HexNAc) and the absence of a fragment ion at *m/z* 606 (corresponding to loss of methanol from *m/z* 638) which would be present if the 3-position of the HexNAc were unsubstituted. Further evidence for the branch assignments were provided by data from hydrofluoric acid treatment (Figure 9C) and subsequent exo-β-galactosidase digestion (Figure 9D). Hydrofluoric acid treatment is known to remove fucose residues linked at the 3-position of GlcNAc, and the fucose attached to the 6-position of the proximal GlcNAc of the chitobiose core is largely unaffected by this treatment (Sutton-Smith *et al.*, 2000). The major signal at *m/z* 2593 (Figure 9B) shifts to *m/z* 2245 (loss of two fucose residues; Figure 9C) and to *m/z* 1836 (loss of two galactose residues Figure 9D) after hydrofluoric acid treatment and exo-β-galactosidase digestion, respectively, data that are totally consistent with the presence of two Lewis^x antennae. Further evidence for the Lewis^x antennae was provided by GC-MS linkage analysis, which showed a major peak for 3,4-linked GlcNAc that was significantly reduced after hydrofluoric acid treatment concomitant with an increase in 4-linked GlcNAc (Table I).

Evidence for the positions of attachment of the two Lewis^x antennae to the core was also provided by the linkage data. Thus the intact glycans were rich in 2-Man, 3,6-Man, and 3,4,6-Man together with a small amount of 2,4-Man and a trace amount of 3-Man (Table I). Significantly, the absence of 2,6-linked and 6-linked mannose rules out structures carrying a branch at the 6-position of the 6-arm. Thus the only possible sites for branch attachment are the 2- and 4-positions of mannose. The very low abundance of 2,4-mannose suggested that the major component (*m/z* 2593, Figure 9B) contains little if any nonbisected N-glycan with two Lewis^x-bearing branches linked at the 2- and 4-positions of the 3-linked mannose arm of the core. After exo-α-mannosidase treatment the level of 3,6-Man was markedly reduced, indicating that this component was mostly derived from high mannose structures that are also present in the glycan mixture (see Figure 9 legend). Significantly, 2-Man and 3,4,6-Man were similarly abundant in the exo-α-mannosidase treated sample (Figure 9E), suggesting that the two branches of the major component are attached on the 3-arm and at the bisecting position, respectively.

Nano-electrospray tandem mass spectrometry (MS/MS) experiments on selected molecular ions in the spectra from the hydrofluoric acid– and exo-β-galactosidase–treated samples provided confirmation for the two branches being linked to separate mannose residues. Thus, collisional activation of the major defucosylated product at *m/z* 1134 $[M+2Na]^{2+}$ (corresponding to the singly charged ion at *m/z* 2245 in the FAB spectrum shown

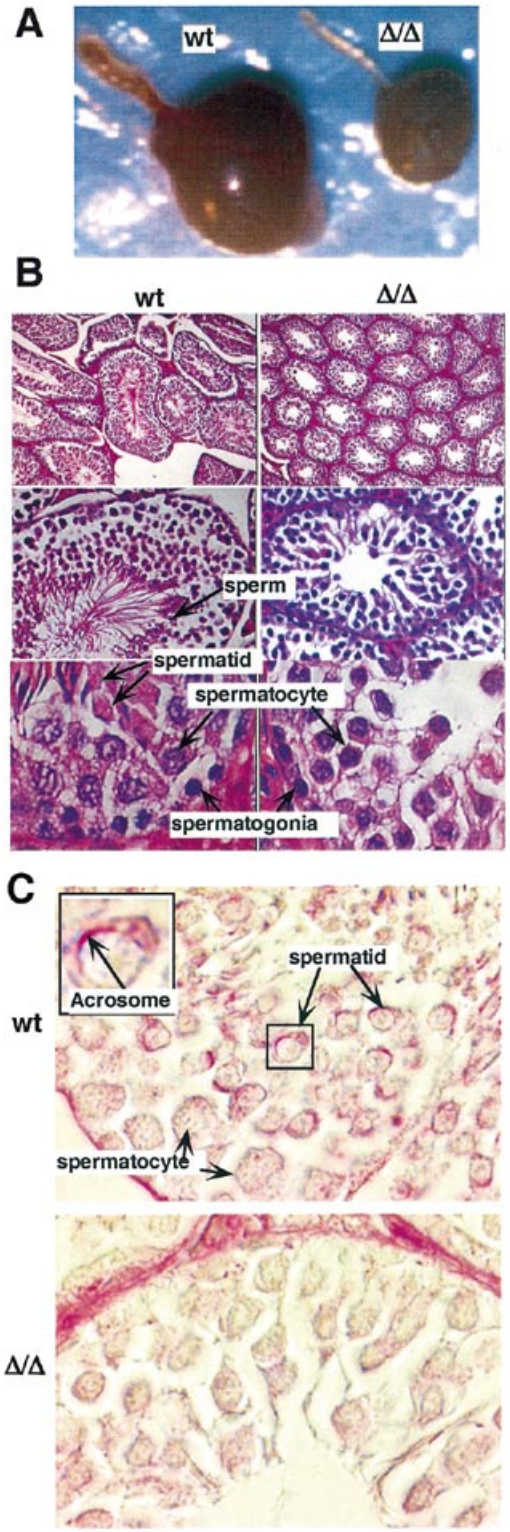

Fig. 8. Survival of *Mgat2*-null mice precludes reproduction in males due to spermatogenic failure. (**A**) Testes from mice lacking the *Mgat2* gene (right) are approximately one-third the size of a wild-type littermate (left). The photograph shows a representative testis (102 mg) of a wild-type male at the age of 3 months with the testis of its *Mgat2*-null littermate (37 mg). (**B**) The spermatogenic differentiative series is revealed by histochemical analyses with hematoxylin/eosin staining. Upper panels, 100×; middle panels, 400×; lower panels, 1000×. Loss of spermatids and mature sperm is evident in the *Mgat2*-null testis. (**C**) This is confirmed by absence of the acrosomal cap produced on spermatids using PAS staining (1500×).

in Figure 9C) gave a singly charged ion at *m/z* 1576 and a doubly charged ion at 800 consistent with loss of Hex-HexNAc-Hex from the intact molecule, indicating that the two defucosylated branches are not attached to the same mannose. Similarly, HexNAc-Hex was liberated on collisional activation of the exo-β-galactosidase product at *m/z* 1836 (see Figure 9D), which can only occur if the Hex is singly substituted with HexNAc.

These findings confirm the presence of a novel N-glycan structure with a branch on the bisected GlcNAc, as represented in Figure 9F. No other branch arrangements are consistent with the linkage data, in particular the relative abundance of 2-Man and 3,4,6-Man (Figure 10E), the MS/MS data, and the overall composition. The resistance of this glycan to jackbean exo-α-mannosidase digestion, as revealed by FAB-MS experiments and by the lack of 3,4-Man in the linkage data of the digestion products (Figure 9E), is fully consistent with previous work on bisected N-glycans (Sutton-Smith *et al.*, 2000; Chui *et al.*, 2001). Furthermore, the data support the other assignments shown in Figure 9B–D, including the two Lewis^x branches attached at positions 2 and 4 of the 3-arm of the core (*m/z* 3216). N-glycan structures in the brain did not show major signals suggesting this novel N-glycan branch, although there was a minor signal at *m/z* 2593, which is likely to correspond to the novel bisected branch structure observed in the kidney (not shown).

Defective lymphocyte ontogeny and autoimmune pathogenesis

Genetic defects in N-glycan branching have been found to alter immune function with pathologic consequences (Chui *et al.*, 2001; Demetriou *et al.*, 2001). Although normal numbers and frequencies of white blood cells were present in peripheral blood of *Mgat2*-null mice, alterations of lymphocyte development and cellularity were noted among primary and secondary lymphoid organs (Figure 10A,B). T cell development in the thymus was attenuated in about half of cases, with 20% of normal thymocyte numbers and a severe reduction in the level of mature T cell precursors—the $CD4^+CD8^+$ thymocytes (Figure 10A,B). Reduced numbers of lymphoid cells were also noted in the spleen. In addition, an increase in erythroblasts was observed with splenomegaly, as also found in αM-II null mice (Chui *et al.*, 1997; data not shown). Reduced cellularity was also evident in the bone marrow of these same *Mgat2*-null mice due to lower numbers of B lymphocytes in the presence of normal levels of myeloid and erythroid lineages (Figure 10A). Defective B cell differentiation was detected in the bone marrow by a reduction in the numbers of IgM^+IgD^- pre-B cells (Figure 10B). However, this defect was not a complete block because normal numbers of B cells with nominal cell surface activation and differentiation markers were observed among *Mgat2*-null survivors (Figure 10A). However, the lymph nodes of one third of 6–9-month-old *Mgat2*-null mice were enlarged with increased numbers of T cells present, suggesting an ongoing infection and potentially aberrant immune response (data not shown).

Glomerulonephritis with immunoglobulin deposition was observed on histologic examination of the kidneys of all *Mgat2*-null survivors more than 6 months of age (Figure 10C). The severity increased with age, and by 9 months extensive mesangial expansion was noted that frequently occluded the lumen of glomerular capillaries. Mononuclear cell infiltrates

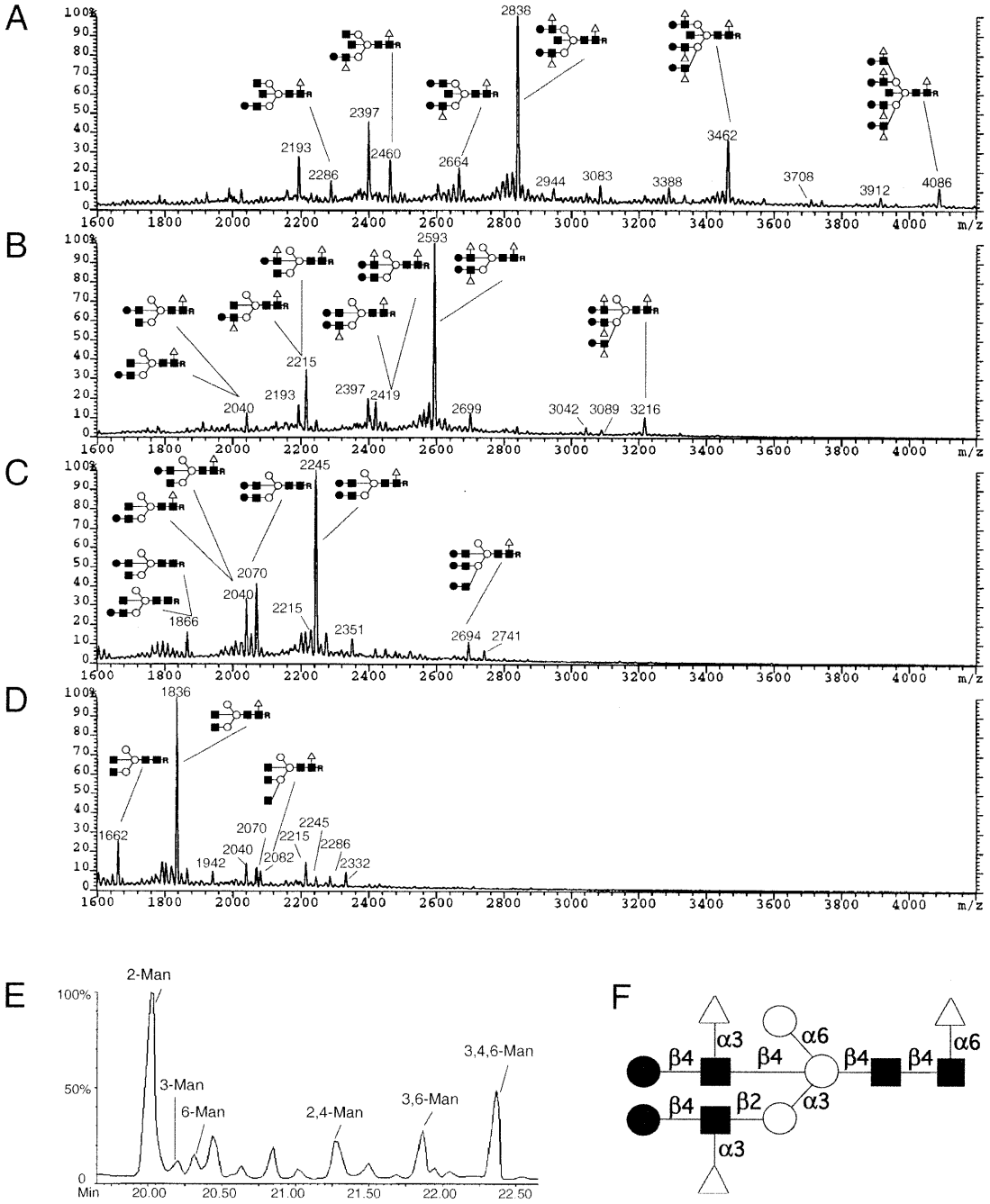

Fig. 9. Hybrid N-glycans predominate and novel N-glycan branch biosynthesis occurs in the absence of *Mgat2*. (**A**) The high mass FAB spectrum of the PNGase F released permethylated N-glycans from wild-type mouse. (**B–D**) High mass FAB mass spectra of permethylated N-glycans from *Mgat2*-null mouse kidney after successive sequential degradation experiments: (**B**) The FAB spectrum of the PNGase F released permethylated N-glycans. Signals at *m/z* 2193 and 2397 are attributed to high mannose structures. (**C**) The FAB spectrum after exo-α-mannosidase digestion and hydrofluoric acid treatment. (**D**) The FAB spectrum after further digestion with exo-β-galactosidase. All molecular ions are sodiated species. Signals at *m/z* 2944 (panel **A**), *m/z* 2699 and 3089 (panel **B**), *m/z* 2351 and 2741 (panel **C**), and *m/z* 1942 and 2322 (panel **D**) are artifacts of the FAB analysis. Other minor unassigned signals correspond to varying degrees of truncation of the assigned structures. Black square, N-acetylglucosamine; open triangle, fucose; black circles, galactose; open circles, mannose. *R* denotes the position of the asparagine residue prior to release of N-glycans by PNGase F from trypsinized detergent extracts of homogenized organs. (**E**) Partial total ion chromatogram of linkage data from the exo-α-mannosidase digested PNGase F released N-glycans from *Mgat2*-null mouse kidney. The minor 6-Man peak was not observed prior to exo-α-mannosidase digestion. Several of the partially methylated alditol acetates have coeluting noncarbohydrate contaminants as revealed by their mass spectra. Hence, mass spectral ion counts rather than the total ion counts were used for quantitative purposes. (**F**) Proposed structure for the major N-glycan present in *Mgat2*-null kidney.

were also observed in some cases (data not shown). Blood in the urine was visible in some aging *Mgat2*-null survivors, and urinalysis revealed moderate to severe proteinuria in almost all *Mgat2*-null survivors (Figure 10D). Increased serum titers of

Table I. GC-MS linkage analysis of partially methylated alditol acetates obtained from N-glycans released by PNGase F digestion from a *Mgat2*-null mouse kidney

Elution time (min)	Diagnostic fragment ions	Assignment	Relative abundance[a]
17.19	117, 131, 175	t-Fuc	0.97
18.78	102, 118, 129, 145, 161, 162, 205	t-Man	1.24
19.08	102, 118, 129, 145, 161, 162, 205	t-Gal	0.68
20.02[b]	129,130, 161, 234	2-Man	1.00
20.32	118, 129, 161, 234	3-Man	0.04
21.27	113, 173, 190, 233	2,4-Man	0.14
21.88[b]	118, 129, 189, 234	3,6-Man	0.42
22.37[b]	118, 333	3,4,6-Man	1.00
22.95	117, 159, 203, 205	t-GlcNAc	0.11
23.90	117, 159, 233	4-GlcNAc	1.92
24.80[c]	177, 159, 346	3,4-GlcNAc	2.27
25.30	117, 159, 261	4,6-GlcNAc	0.25

[a]Relative abundance is based on the total ion current of each partially methylated alditol acetate spectrum.
[b]After exo-α-mannosidase digestion 3,6-Man is significantly reduced while the relative abundance of 2-Man and 3,4,6-Man remain similarly abundant.
[c]After hydrofluoric acid treatment 3,4-GlcNAc is significantly reduced.

autoantibodies were detected, indicating an autoimmune component of disease due to GlcNAcT-II deficiency (Figure 10E). Several *Mgat2*-null mice were found to have increased bacterial titers in the gut and extensive kidney tubule dilation, suggesting the possibility of pyelonephritis in some cases (data not shown).

Discussion

We have investigated the outcome of introducing a homozygous null deletion of the *Mgat2* gene into the mouse germline and compared our findings with those from clinical studies of patients with an identical glycan biosynthetic defect responsible for CDG-IIa disease. The aforementioned features of oligosaccharide synthesis as governed by glycosyltransferases in the Golgi apparatus (see *Introduction*) have implied that different phenotypic and disease profiles may occur among mammalian species bearing the same genetic defect in glycan formation. However, we have found considerable similarities involving functional deficiencies of specific glycoproteins and physiologic systems among humans and mice lacking the *Mgat2*-encoded GlcNAcT-II glycosyltransferase. Ontogenic and homeostatic functions for complex N-glycans were noted, and genetic modifiers of disease severity were detected in the mouse genome. The future identification of these modifiers should be informative by further revealing molecular mechanisms employed by N-glycans in the modulation of mammalian physiology and disease pathogenesis.

Differences observed in disease signs between humans and mice with GlcNAcT-II deficiency may indeed reflect species-specific functions of complex-type N-glycans, especially in examples where human CDG-IIa disease signs were not observed in the mouse. However, disease signs not reported in human CDG-IIa but present in *Mgat2*-null mice may be prognostic for human patients with age, as all CDG-IIa patients are children as of this writing. It is also possible that humans most severely affected may die in gestation or in early postnatal life, whereas those least affected may reach maturity with a variable subset of disease signs. Although human *MGAT2* mutations thus far analyzed appear to completely disable enzymatic activity *in vitro* (Tan *et al.*, 1996), heterogeneity in disease signs may also result from varied and low residual activity of mutant human GlcNAcT-II not detectable by current assays. Nevertheless, the remarkable degree of conservation in disease signs between humans and mice with GlcNAcT-II deficiency can now be considered alongside results of other mutations in the mammalian germ line that block adjacent steps in N-glycan biosynthesis to further establish structure–function relationships involving specific glycosyltransferases and N-glycan branches.

Branch-specific N-glycan formation and function in mammals

The completion of embryonic development in the absence of *Mgat2* gene function contrasts with results obtained in studies of *Mgat1*-null embryos. Loss of *Mgat1*-encoded GlcNAcT-I activity disables production of hybrid N-glycans; instead, only high-mannose types are produced. The resulting absence of both hybrid and complex N-glycan formation ablates all N-glycan branching as initiated by N-acetylglucosamine linkages and invariably results in intrauterine embryo death during E9 of ontogeny (Ioffe and Stanley, 1994; Metzler *et al.*, 1994). This period in embryonic development represents the first trimester in human development and is a time when cell type–specific interactions and signaling processes promote significant morphogenic events. *Mgat1*-null embryos are defective in neural tube development, vascularization, and exhibit a randomization of cardiac loop formation resulting a high frequency of *situs inversus* of the early heart. No examples of human *Mgat1* mutation or GlcNAcT-I deficiency have been reported. Hybrid-type N-glycans therefore appear to represent the minimal biosynthetic N-glycan structural repertoire necessary for mammalian ontogenic processes that enable, in at least most cases, the completion of embryogenesis. However, this

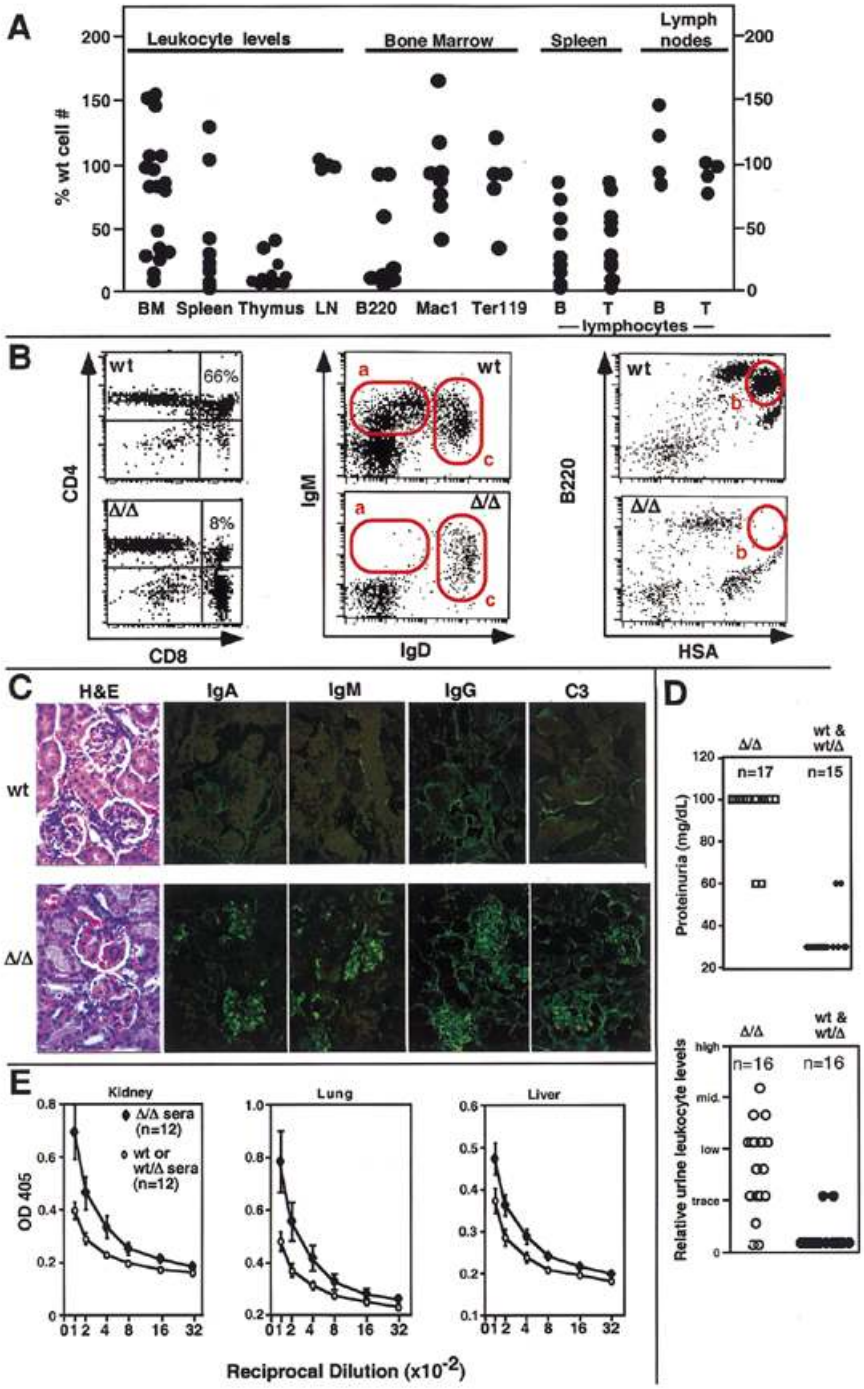

Fig. 10. Immune ontogenic dysregulation with glomerulonephritis in aging *Mgat2*-null mice produced in the ICR background. (**A**) Leukocyte numbers were reduced in the spleen. T cells were deficient in the thymus, and fewer B cells ($B220^{+}$) were observed in the bone marrow. Myeloid (Mac1) and nucleated erythroid (Ter119) cell numbers appeared normal. T, T cells; B, B cells. The number of mice analyzed are listed from left to right in the same order as in the panel: $N = 17$, 9, 12, 4, 9, 9, 5, 11, 12, 4, 4. Each filled circle represents measurement from a different mouse. (**B**) Thymocyte development was altered with fewer T cell precursors ($CD4^{+}CD8^{+}$) (left panel). In the marrow of *Mgat2*-null mice, a reduction in subpopulation of immature B cells ($IgM^{+}IgD^{-}$) ($B220^{+}HSA^{hi}$) is noted (gates a and b). Mature B cells are generated in reduced numbers (gate c). (**C**) Comparison by hematoxylin/eosin staining of wild-type kidney glomeruli (upper left panel) with those from *Mgat2*-null mice indicates signs of glomerulonephritis with mesangial involvement (lower left panel). Glomeruli of *Mgat2*-null mice contain increased levels of IgA, IgM, IgG, and C3 deposits (right panels). Magnification: 400×. (**D**) Urinalysis indicates proteinuria (upper panel) and leukocyturia (lower panel). (**E**) Self-reactive antibodies to autologous protein from kidney, lung, and liver are increased in the circulation of *Mgat2*-null mice.

hybrid N-glycan repertoire is inadequate for the normal development and function of various physiologic systems, resulting in CDG-IIa.

Human and mouse embryos appear able to complete embryonic development and survive past birth in the absence of *Mgat2* gene function. The frequency of homozygous *Mgat2*-null

mouse embryos at day 15 was slightly less than normal (17% in over 500 offspring analyzed) and tissues were deficient in PHA lectin binding by embryonic day 10 (data not shown). It therefore is likely that some mouse embryos lacking *Mgat2* are more severely affected and die *in utero*. Whether we analyzed embryos or postnatal mice, we found by using lectin histology that complex N-glycans were similarly deficient from *Mgat2*-null tissues in all cases (data not shown).

Curiously, low levels of GlcNAcT-II activity and complex N-glycans were observed in the intestine, a finding that requires further investigation. Some of this activity may be due to the presence of GlcNAcT-III and/or GlcNAcT-IV in the *in vitro* assays performed. However, we cannot rule out the presence of an unknown GlcNAcT-II isozyme. Structural analyses of the products formed in the intestine are required to resolve this issue, as was accomplished in the kidney. Finally, it remains possible that the origin of this enzyme activity toward the synthetic substrate is nonmammalian, perhaps bacterial. Thus far, however, no bacterial homologues of GlcNAcT-II have been detected in the DNA databases.

N-glycan branching in the absence of Mgat2 function

Mgat2-encoded GlcNAcT-II deficiency results in an altered structural repertoire of N-glycans with a deficiency in complex subtypes. Also as expected, GlcNAcT-II deficiency results in an increase of hybrid-type N-glycan branches due to the underlying activities of both *Mgat1* gene-encoded GlcNAcT-I activity and an alpha-mannosidase-III activity acting on the $Man_5GlcNAc_2$-Asn N-glycan substrate in N-glycan synthesis. Extensive glycan analyses were performed on the kidney because the initial screening suggested the presence of unusual structures. Unexpectedly, the major glycan identified in the kidney carries a $Lewis^x$ antenna at the bisecting position (Figure 9F). This structure has not been previously identified in bisected N-glycans as they have been shown to exist with an unsubstituted bisecting GlcNAc residue.

Whether this novel N-glycan branch structure exists in appreciable levels among tissues and cell types from wild-type mammals will require further study. We consider it possible that the bisecting GlcNAc in wild-type derived N-glycans is inaccessible to one or more Golgi-resident galactosyltransferases that may be preferentially expressed in the kidney. In the absence of GlcNAc addition on the 6-arm mannose residue, these N-glycans may become substrates of such galactosyltransferase activity. This could reflect a physiologically relevant mechanism that generates N-glycan branches and terminal glycan linkages in situations where GlcNAcT-II is scarce or absent. Expression levels of GlcNAcT-II may thus be relevant in some cases; in this regard it is interesting to note that the highest levels of *Mgat2* RNA expression occur in tissues highly dysfunctional in the absence of GlcNAcT-II.

The bisected branch structure observed in *Mgat2* deficiency could be considered a novel "pathway," or perhaps a "kinetic artifact"; however, the more relevant issue is perhaps whether this structure in some way modulates physiologic and disease processes. This possibility may be addressed, in one manner, by analyzing the disease course in mice lacking both *Mgat2* and *Mgat3* genes. N-glycan branching itself may be highly essential in providing a means to generate multivalent glycan ligands for various endogenous lectin molecules. Alternatively, unique saccharide linkages and termini produced on a subset of N-glycan branches may engender specific and critical functions that cannot be synthetically duplicated on other branches.

Mouse and human CDG-IIa

A tabulated comparison of mice and humans that are deficient in GlcNAcT-II activity most clearly indicates significant conservation of complex N-glycan function (Table II; Jaeken *et al.*, 1994; Engelhardt *et al.*, 1999; Cormier-Daire *et al.*, 2000). Failure to thrive with dysmorphic facial features and poor psychomotor development are common to both species lacking GlcNAcT-II. Human patients have been found to suffer epileptic seizures, and we noted that some mutant mice exhibited tremors and intermittent paralysis. Both species have normal cerebellar development. Moreover, brain anatomy in the mouse appeared unremarkable without evidence of neuronal or glial cell loss. Deep tendon reflexes, nerve conduction velocities, and evoked potentials in human CDG-IIa are normal and mutant mice exhibited normal synaptic transmission in spontaneous and evoked neuromuscular recordings.

Osteopenia with thoracolumbar kyphoscoliosis was also common to both species. Studies of bone formation and resorption processes in the mouse yielded insights involving this phenotype, which manifests as a delayed induction of secondary ossification centers and a 30% reduction in bone density with poor joint articulation and fractures common. The increased osteoclast activity occurred without a concomitant increase in osteoblast activity, indicating enhanced bone resorption is involved in causing osteopenia. Moreover, this pathologic osteogenic profile could contribute substantially to the severe locomotor abnormalities observed.

Testicular atrophy is also present in both humans and mice lacking *Mgat2* gene function. Whether human males with CDG-IIa are fertile is not yet known; however, male *Mgat2*-null mice were invariably infertile with a defect in spermatocyte differentiation leading to an absence of spermatids and sperm. We predict that human males with CDG-IIa will also be found to be infertile and similarly aspermatic, reflecting a conserved spermatocyte differentiation event that requires complex N-glycans on one or more glycoproteins for male gamete development and viability.

Further insights into complex N-glycans in normal and disease processes were obtained from studies of blood coagulation, blood chemistry, gastrointestinal function, and the immune system. Blood coagulation factor deficiencies revealed a profile very similar to human CDG II-a and suggesting a tendency towards thrombosis. These findings imply that complex N-glycan branching in the liver is crucial in the production or stability and half-life of specific coagulation factors in circulation. These alterations could be especially relevant in situations where organ dysfunction produces excessive stress on cellular membranes, such as that observed in the gastrointestinal tract.

The diagnosis of volvulus and obstipation in human CDG-IIa indicates abnormalities in gastrointestinal function. Mice lacking *Mgat2* were affected with obstipation, constipation, hemorrhage, and rectal prolapse. Volvulus was not detected in the mouse but may have been present prior to necropsy. Remarkably, a deficiency of intestinal mucin among Brunner's and pyloric glands was noted. The extent of mucin deficiency directly correlated with the frequency of hemorrhage and rectal prolapse (not shown). These results indicate that gastrointestinal

Table II. Human CDG-IIa and the mouse model: diagnosis and phenotypic comparisons

Human	Mouse
Clinically screened by serum transferrin isoelectric focusing. *Loss of E-/L-PHA binding can be substituted (this study)	Biochemically identified by serum transferrin isoelectric focusing or loss of E-/L-PHA lectin binding*
Absence of GlcNAcT-II glycosyltransferase activity in fibroblasts and leukocytes	Absence of GlcNAcT-II glycosyltransferase activity among various tissues, some activity in intestine
Deficiency of complex N-glycans in fibroblasts, lymphoblasts and serum glycoproteins	Deficiency of complex N-glycans from all tissues surveyed, low levels possible in intestines
Failure to thrive	Runted with low post-natal survival frequency
Osteopenia	Osteopenia, joint defects, increased osteoclast activity
Thoracolumbar kyphoscoliosis	Thoracolumbar kyphoscoliosis
Dysmorphic facial features	Dysmorphic facial features
Severe psychomotor retardation	Defective locomotor function and muscular strength
Normal cerebellar development	Normal cerebellar and Purkinje cell development
Normal deep tendon reflexes	Normal neuromuscular synaptic transmission
Epilepsy	Tremors and seizures common in some mice
Stereotypical hand-washing behavior	Excessive barbering and circling behavior
Mental retardation	Tests in ICR strain background inconclusive
Blood coagulopathy with increased APTT (15%), and reductions in factors VII (57%), XI (30%,40%), XII (73%), antithrombin-III (43%), and protein C (30%,62%)	Blood coagulopathy with increased APTT (13%), and reductions in Factors VII (65%), XI (40%), XII (80%), antithrombin-III (20%), and protein C (40%)
Testicular atrophy, infertility likely	Testicular atrophy and spermatogenic failure
Occasional ventricular septal defect of the heart	One case of ventral septal defect of the heart
Low serum IgG levels	Partial block in pre-B cell development, reduced, levels of B cells, varied serum Ig levels
Splenomegaly	Splenomegaly
Normal hemogram	Minor to moderate anemia, reduced platelet levels
Hepatomegaly	Not observed in the mouse
Obstipation and volvulus	Obstipation, constipation, rectal prolapse. Reduced mucin levels, Brunner's gland abnormalities and hemorrhage
High AST, normal ALT; normal to slightly reduced serum protein levels	High AST, normal ALT; reduced serum glucose and Ca^{2+}; slightly reduced serum protein levels
Susceptibility to infection	Bacterial overgrowth in the gut, pyelonephritis possible, glomerulonephritis, and autoimmune disease

*Transferrin isoelectric focusing is not diagnostic in all human CDG cases. Blood coagulopathy and factor deficiency profiles can be suggestive. Loss of E- or L-PHA lectin binding detects absence of *Mgat2* function in mouse and human blood or tissue samples.

dysfunction in the absence of complex N-glycans may be a result of mucin deficiency, leading to defects in food transport, reduced blood glucose, reduced serum protein levels, and mucosal injury with hemorrhage exacerbated by the blood coagulopathy observed. How complex N-glycans act to promote mucin production is unclear at this time. In further comparisons, blood chemistry indicated a remarkably similar, and aberrant, AST/ALT profile among mice and humans. These results are not consistent with significant liver dysfunction but suggest hemolytic disease, possible pulmonary embolisms, and muscle damage.

Some phenotypic findings in the mouse were dissimilar to human CDG-IIa or infrequent in occurrence. Heart development appeared normal in the *Mgat2*-null mouse in all but one case of ventricular septal defect (not shown); however, ventricular septal defect has been found in two of the four currently identified human patients. Additionally, mutant mice were anemic with an increase in reticulocytes and a decrease in platelets. However, peripheral blood indices are reported to be normal in human CDG-IIa patients. An essential role for complex N-glycans in human erythropoiesis and erythroid function is thus not indicated, in contrast to mice lacking alpha-mannosidase-II or GlcNAcT-II. Hepatomegaly also was not observed among *Mgat2*-null mice, although it has been reported in human CDG-IIa. Differences in human and mouse CDG-IIa also appear to involve serum Ig production. Low levels of serum Ig have been described in CDG-IIa patients and suggest defective B cell development or function. Although Ig levels vary in the ICR strain background, and thereby complicate this analysis, those *Mgat2*-null mice studied did not harbor significantly reduced levels among survivors more than 6 weeks of age (data not shown).

Lymphopoiesis and immune function are, however, susceptible to loss of *Mgat2* gene function. A block in pre-B cell differentiation

was observed in the *Mgat2*-null mouse bone marrow, leading to depressed B cell numbers. T cell development in the thymus was also defective, with fewer thymocytes and mature T cell precursors present. However, these developmental defects were only partial (and perhaps temporal) in scope because peripheral lymphoid compartments were colonized with mature B and T cells in these same animals. No effect was seen on myeloid development or on cell viability. Human CDG-IIa patients are, however, prone to infections; we noted a substantial increase in bacterial titers in the gastrointestinal tract of some *Mgat2*-null mice. Cultures of these bacteria failed to indicate the presence of abnormal strains among mice house in a specific pathogen-free vivarium; however, yeast were found on occasion.

Kidney dysfunction and autoimmune involvement were suspected in aging *Mgat2*-null mice following the detection of proteinuria. Recent findings of systemic lupus erythematosus–like autoimmune disease in alpha-mannosidase-II deficient mice (Chui *et al.*, 2001) may therefore be recapitulated in *Mgat2*-deficient disease, considering the adjacent downstream position of GlcNAcT-II in the N-glycan biosynthetic pathway. We found increased autoantibody titers in the serum of *Mgat2*-null mice. However, the degree of this increase was less than that noted in alpha-mannosidase-II deficient mice. An attenuation of the autoimmune disease phenotype would not be expected simply from the positions of alpha-mannosidase-II and GlcNAcT-II in N-glycan biosynthesis; however, systemic loss of all complex N-glycans only occurs with *Mgat2* deficiency, and this could moderate the autoimmune disease component. For example, lymphocyte development and immune responses appear normal in alpha-mannosidase-II deficiency because the alternate pathway to complex N-glycans remains intact (Chui *et al.*, 2001). Future studies of lymphocyte immune function in the absence of *Mgat2* may be informative in this regard. Moreover, *Mgat5*-deficient mice that lack one branch found in complex N-glycans, the formation of which depends on GlcNAcT-II function, have been described as hyperresponsive to immune stimuli (Demetriou *et al.*, 2001). The oldest CDG-IIa patient is presently 19 years of age, and no CDG-IIa patient has been reported thus far with glomerulonephritis, kidney dysfunction, or signs of autoimmune disease.

GlcNAcT-II glycosyltransferase as a biological modifier

Altered survival frequencies and disease penetration among *Mgat2*-null mice suggest a modulatory role for GlcNAcT-II and complex N-glycans in physiology. The severity of the disease in the mouse was significantly reduced when the mutation was bred into a distinct genetic background (the ICR strain). Survival frequencies from breedings undertaken indicated the presence of autosomal genetic modifiers unlinked to the *Mgat2* gene in meiotic recombination. The relevance of this finding to human CDG-IIa is uncertain since the survival frequency of newborn humans with *MGAT2* gene defects is unknown. All CDG-IIa cases have been diagnosed only after several years of postnatal life, and some clinical heterogeneity is present among CDG-IIa patients. Heterogeneity may also result from the presence of currently unknown mutations in *MGAT2* that alter but don't fully disable GlcNAcT-II activity. Nevertheless, long-term mouse survivors may reflect those children that have survived early postnatal development but failed to thrive, were subsequently diagnosed, and are currently in clinical care. Should human genetic modifiers of CDG-IIa disease exist and cause variations in disease penetrance, a proportion of the human population with CDG-IIa may well be undiagnosed at this time. In this regard, recent measurements of allele frequencies among some European populations suggest that some forms of CDG-I are more common than are clinically recognized (Matthijs *et al.*, 2000). Additionally, diagnosis by aberrant transferrin isoelectric focusing is not always a reliable indicator (Knopf *et al.*, 2000), further underscoring the view that CDG prevalence in the human population is not yet established (Kornfeld, 1998; Freeze, 1998).

Heterogeneity in human CDGs illustrates the modulatory nature of N-glycan functions in physiology. Even among those patients with the same mutations, CDG-I phenotypes are clinically heterogeneous, and tissue-specific alterations of N-glycans in CDGs have been reported (Dupré *et al.*, 2000; Imtiaz *et al.*, 2000; De Lonlay *et al.*, 2001). How might this heterogeneity be produced? Factors affecting efficiency of protein N-glycosylation could be involved and contribute to what has been termed microheterogeneity of protein glycosylation. Obviously, the known depressive affect of alcohol ingestion on liver protein N-glycosylation has been the basis for the use of the serum transferrin isoelectric focusing to detect CDGs. However, endogenous factors that affect the frequency of site-specific protein glycosylation and that might thereby regulate glycoprotein function in normal contexts have not been identified at this time. Alternatively, genetic polymorphisms among substrates may also be considered. For example, gene mutations that alter peptide sequences to include or exclude an N-glycosylation site could retain glycoprotein expression while modulating physiologic function. Such alterations in glycan formation or structure can affect glycoprotein half-life, aggregation properties, and lectin-ligand binding—all of which represent mechanisms capable of modulating signal transduction events in biologic processes.

The physiologic systems defective in *Mgat2* null mice were not completely disabled but instead functioned less effectively and, in some cases, aberrantly. Nevertheless, disease was typically severe and lethality was common. This is consistent with the functional theme of Golgi-produced complex N-glycans as signal modulators that alter the flow of information between viable cells. Our findings further indicate that the mouse can provide an accurate model of human disease resulting from a genetic defect in protein N-glycosylation. In this regard, efforts to increase mucin production in the gastrointestinal tract, retard bone resorption, and normalize hematologic parameters may be useful approaches in treating CDG-IIa. A curative approach however may ultimately require gene replacement therapy, unlike some CDG type I syndromes that can be treated by the addition of specific monosaccharides to the diet (Niehues *et al.*, 1998; Marquardt *et al.*, 1999). In CDG-IIa, there are no deficiencies of monosaccharide donors or other building blocks in glycan metabolism. With more study and with the production of other CDG models, we are optimistic that an increase in information pertinent to CDG pathogenesis will ensue and facilitate the development of additional effective therapeutic approaches.

Materials and methods

Northern blot analysis

Total RNA was prepared from mouse tissues and subjected to 1% formaldehyde denaturing agarose gel electrophoresis. The blot was analyzed using a mouse *Mgat2* coding sequence probe by procedures previously described (Shafi *et al.*, 2000).

Mgat2 cloning and gene targeting

A human genomic *Mgat 2* probe was used to isolate two overlapping clones from a mouse 129/*SvJ* genomic library and to construct a targeting vector. ES cell clones bearing both systemic and conditional deletions of the *Mgat2* gene were obtained as described (Marth, 1996). To acquire offspring bearing the null mutation, chimeric mice were generated by microinjection of ES cells into C57BL/6 blastocyst-stage embryos and were bred to ZP3-Cre transgenic mice maintained on the C57BL/6 background for more than 10 generations. The mutations were further bred into the C57BL/6 or ICR strains (HSD) as described in the text.

GlcNAcT-II activity

Extracts for GlcNAc-T II assays were obtained by homogenizing tissues in buffer containing 2% Triton X-100 in the presence of protease inhibitors. GlcNAc-T II activity was assayed in 0.75 mM [Man(alpha1-6)][GlcNAc(beta1-2)Man(alpha1-3)]Man(beta-1-O)octyl (GnM3-octyl) (Dr. Hans Paulsen, Hamburg, Germany), 1.0 mM UDP-[^{3}H]GlcNAc (6700 dpm/nmole), 12.5 mM AMP, 0.15 M GlcNAc, 0.1 M MES (pH 6.5), and 20 mM $MnCl_2$ in a total volume of 20 µl for 30–60 min at 37°C. Product formation was assayed with Sep-Pak C18 reversed phase cartridges as previously described (Metzler *et al.*, 1994). GlcNAcT- I was assayed as for GlcNAcT-II except that the substrate was 0.50 mM [Man(alpha1-6)][Man(alpha1-3)]Man(beta-1-O)octyl (M3-octyl) (Dr. Hans Paulsen, Hamburg, Germany) and the incubation contained 0.125 M GlcNAc. All assays were done at least in duplicate.

Histology

Tissues were frozen in Optimal Cutting Temperature medium (VWR Scientific) by placing embedded samples in a dry ice/isopentane bath and sectioned at 5 µm. Bone was reacted for TRAP activity (Sigma, Cat.387). Lectin histochemistry was performed as previously described with some modification (Metzler *et al.*, 1994; Priatel *et al.*, 2000). Briefly, tissue sections used for L-PHA staining (E-PHA not shown) were treated in 0.03% H_2O_2 in methanol for 20 min, then blocked by 1% bovine serum albumin (BSA) in phosphate buffered saline for 30 min and incubated with 10 µg/ml of biotinylated L-PHA and Conacavalin A (Vector) for 4 h. Lectin binding was detected by horseradish peroxidase/Strepavidin (Vector, ABC kit) with diaminobenzidine substrate (Calbiochem). For immunofluorescence, the sectioned tissues were stained with fluorescein isothiocyanate (FITC)–conjugated goat anti-mouse antibody specific to IgA, IgM, IgG, and C3 as described elsewhere (Chui *et al.*, 2001). Alizarin and alcian blue staining of cartilage and bone was accomplished as described (Hogan *et al.*, 1994). For hematoxylin and eosin staining, the tissues were fixed, embedded, and sectioned at 7 µm as described (Chui *et al.*, 2001). Prior to hematoxylin and eosin staining, long bones were decalcified and fixed in Cal-EXI™II (Fisher) for 48 h. Whole blood analysis by E-PHA binding was accomplished by blotting 5 µl on nitrocellulose and allowing the blot to dry for 30 min prior to adding biotinylated E-PHA or L-PHA (Vector) at 2 µg/ml in Tris-buffered saline (TBS, pH 7.5). Following 3× washes in TBS, binding was detected with chemiluminesence or colorimetric detection reagents as above.

Mass spectrometry

N-glycans were isolated from trypsinized detergent extracts of homogenized organs by peptide:N-glycanase F (PNGase F) treatment and subjected to hydrofluoric acid defucosylation and digestion with various exoglycosidases before analysis by FAB-MS and GC-MS as previously described (Sutton-Smith *et al.*, 2000). Nano-electrospray-MS/MS was carried out on the Q-TOF as described previously (Teng-umnuay *et al.*, 1998) using collision energies in the range 50–100 eV.

Locomotor and muscular function

To assess locomotor gait, each paw was coated with different color ink and the mouse was allowed to walk through a 9 cm × 35 cm × 6 cm opaque tunnel placed on a sheet of paper (Barlow *et al.*, 1996). For the rotarod test, mice were placed on an accelerating (4–40 rpm over 5 min) rotating drum (3-cm diameter) for three trials with a minimum of 15 min interval between trials. The mean latency to fall over the three trials was determined. In the wire hang test, mice were allowed to grasp a 1-mm-diameter wire with their front paws and then suspended 40 cm above a padded surface. The mean latency to fall (maximum 60 s) over three trials was determined. To determine grip strength, mice were suspended by the tail and lowered until the mouse grasped the loop of the mouse grip strength meter (UGO Basile, Varese, Italy). Each mouse was then gently pulled away from the loop, and the maximum grip force exerted by the mouse before loosing its grip was recorded. Five trials were run; the mean of the middle three scores was used in the analysis. Student *t*-tests were used to assess the differences between the genotypes.

Nociception

The hot plate and tail flick tests were preformed in a one trial test. The mean of three trials was used as the dependent measure. The latency (30-s maximum) to exhibit either a hind-foot shake or lick after placement on a 55 °C platform was measured. The latency (10 s maximum) for each mouse to move its tail from the path of a bright photo beam was also recorded. Student *t*-tests were used to assess the differences between the genotypes.

Synaptic transmission

Studies used a total of six null, two wild-type, and four heterozygous mice. Ages of animals at study averaged 28 days (range 22–32 days), except for one null/wild-type pair studied at 77 days. Neuromuscular transmission was characterized using the phrenic nerve/diaphragm preparation as described (Hong and Chang, 1989), except that experiments were done at room temperature using physiological Ringer solution consisting of 129 mM NaCl, 5 mM KCl, 2 mM $CaCl_2$, 1 mM $MgCl_2$, 11 mM glucose, and 10 mM Na-PIPES buffer at pH 7.3. Using digitized records, miniature endplate potentials ("minis") were automatically detected and frequency, amplitudes and kinetics analyzed using the program MiniAnalysis (Synaptosoft, Inc.).

Additionally, characterization of the neurally evoked endplate potential ("evoked response") was done on two pairs of null/heterozygote littermates. μ-Conotoxin was used to eliminate muscle contraction when recording these evoked endplate responses (Hong and Chang, 1989).

Hematology and urinalysis

Blood from the tail vein of methoxyfluorane anesthetized mice was collected into EDTA-containing polypropylene microtubes (Becton Dickinson, NJ). Analyses of red blood cells, white blood cells, and platelet cell numbers and morphology were carried out using a Cell-Dyn 3500 Automated Analyzer (Abbott Diagnostics) programmed for mouse blood parameters. Urine was collected and analyzed as previously described (Chui *et al.*, 2001).

Serum chemistry

Blood was collected in the absence of anticoagulants by tail bleed or cardiac puncture and was allowed to clot for several hours in plastic microtubes. The serum was collected by centrifugation. Chemistry analyses were performed using a Beckman CX-7 automated chemistry analyzer with a general CV of <5%.

Coagulation

Nine parts of whole blood collected by cardiac puncture were rapidly mixed with 1 part (v/v) of buffered citrate anticoagulant (0.06 mole/L sodium citrate plus 0.04 mole/L citric acid). Platelet poor plasma (plasma) was prepared from citrated plasma by centrifugation twice at 1800 × *g* for 15 min at 22°C and stored at –75°C. Normal reference mouse plasma (NMP) was prepared by pooling plasma, prepared as above, from 20–30 individual C57BL/6 mice of both sexes. For the one-stage clotting assay, clotting times were determined in duplicates with an ST4 semi-automated coagulation instrument (Diagnostica Stago, NJ). Except as noted below for fibrinogen assay, test samples were diluted in HN buffer (25 mM HEPES, pH 7.5, 150 mM NaCl and 1 mg/ml BSA). The prothrombin time assay was performed by incubating 30 μl of plasma at 37°C for 3 min, followed by the addition of 60 μl of thromboplastin reagent (Thromboplastin C-Plus, Baxter, FL) prewarmed to 37°C to initiate clotting. Activated partial thromboplastin time (APTT) was performed by incubating 30 μl of plasma and 30 μl of APTT reagent (Automated APTT, Organon Technika, NC) at 37°C for 5 min followed by the addition of 30 μl of prewarmed 25 mM $CaCl_2$ to initiate clotting. For the prothrombin (factor II) activity assay, 30 μl of test plasma was diluted 1:20 in HN buffer and incubated for 3 min at 37°C with 30 μl of a 1:1 mixture of human prothrombin-depleted plasma reagent (Diagnostica Stago, Asnieres, France) and rabbit barium-adsorbed plasma. Clotting was then initiated by the addition of 60 μl of thromboplastin C-Plus. Clotting times were converted to percent NMP prothrombin concentration from a log-log standard curve prepared with dilutions between 1:5 and 1:80 in HN-buffered NMP.

Standard curves were prepared on each day of testing. Factor VII and factor X activity assays were carried out identically except that the corresponding human factor–deficient plasmas were used. Factor V activity assay was carried out identically except that 30 μl of a human factor V immunodepleted plasma reagent (American Diagnostica) was used without mixing 1:1 with barium-adsorbed rabbit plasma; the samples were diluted 1:200 in HN buffer; and the standard curves were made with dilutions in HN buffer of NMP between 1:50 to 1:1000. For the Factor VIII activity assay, 30 μl of test plasma was diluted 1:20 in HN buffer and incubated for 5 min at 37°C with 30 μl of human congenital factor VIII–deficient plasma and 30 μl of APTT reagent. Clotting was then initiated with 30 μl of 25 mM calcium chloride. The log-log standard curves were made from NMP diluted 1:5 to 1:80 in HN buffer. The factors IX, XI, and XII activity assays were performed as described for factor VIII assays, except that the corresponding human factor–deficient plasmas were used.

For the fibrinogen clotting activity assay, 60 μl of test plasma, diluted 1:10 and 1:20 in Owren's Veronal Buffer were incubated for 3 min at 37°C followed by the addition of 30 μl of bovine thrombin reagent (Dade Data-Fi thrombin reagent, Baxter, FL) to activate clotting. Clotting times were converted to fibrinogen concentration from a log-log standard curve prepared with dilutions (1:5 to 1:40 in Owren's Veronal Buffer) of standard plasma containing previously calibrated fibrinogen concentrations. The von Willebrand (vWF) antigen assay was peformed in a 96-well microtiter plate precoated overnight at 4°C with 200 μl of 10 μg/ml rabbit anti-human vWF polyclonal antibody (Dako, Denmark) prepared in 50 mM Na_2CO_3, pH 9.6. The wells were then blocked with 25 mM Tris, pH 7.5, 150 mM NaCl (TBS) containing 3% BSA for 2 h at 37°C. After washing several times with TBS containing 1% BSA, 100 μl aliquots of test plasmas, diluted 1:100 and 1:200 in TBS/1%BSA, were incubated in the wells for 2 h at 37°C followed by washing five times with TBS containing 0.05% Tween 20. The wells were then incubated with 100 μl of horseradish peroxidase–conjugated rabbit anti-human vWF polyclonal antibodies (Dako) diluted 1:2000 in TBS/1%BSA for 1 h at 37 °C. After washing again five times with TBS-0.05% Tween 20, the assay was developed using a peroxidase substrate (Bio-Rad, CA) according to the manufacturer's instruction and quantitated at 405 nm using the Versa Max microtiter plate reader (Molecular Devices, CA). A standard curve was constructed with each plate by diluting NMP 1:10 to 1:250 in TBS/1%BSA.

The protein S antigen assay was performed as described for the vWF antigen assay but using polyclonal rabbit anti-human protein S (Dako). For the protein C activity assay, 10 μl of test plasma was diluted 1:20 in TBS containing 100 mM CsCl, were incubated in a microtiter well at 37°C for 15 min with 25 μl of 2 U/ml protein C activator (PROTAC, American Diagnostica, CT) followed by the addition of 25 μl of chromogenic substrate, S-2366, to 2.5 mM (DiaPharma, OH) and absorbance at 405 nm was measured. Absorbances were converted to percent reference mouse plasma protein C from a standard curve prepared with each plate with NMP diluted 1:4 to 1:64 in TBS-CsCl.

For the plasminogen assay, 60 μl of test plasma was diluted 1:60 in 100 mM Tris, pH 8.5, containing 8.3 mM epsilon-aminocaproic acid (EACA) (Calbiochem, CA) were incubated in a microtiter well at 37°C for 5 min. followed by the addition of 20 μl of 2500 Ploug U/ml urokinase (Calbiochem, CA) and further incubation for 60 s. Next, 100 μl of chromogenic substrate, S-2403, 1.2 mM (DiaPharma, OH) were added, and absorbance at 405 nm was measured. Absorbances were converted to percent reference mouse plasma plasminogen from a log-log

standard curve prepared with each plate with dilutions of NMP (1:15 to 1:240) in Tris-EACA buffer. For the alpha-2-antiplasmin assay, 50 µl of test plasma was diluted 1:40 in TBS containing 120 mM methylamine and incubated in a microtiter well at 37°C for 5 min, followed by the addition of 50 µl of 17 µg/ml plasmin (Calbiochem) and incubation for 90 sec. Next, 50 µl of chromogenic substrate, S-2403, 0.75 mM (DiaPharma), were added and residual plasmin activity was measured by absorbance at 405 nm. Absorbances were converted to percent NMP alpha-2 antiplasmin from a standard curve prepared with each plate with dilutions of NMP (1:10 to 1:160) in TBS-methylamine.

For the antithrombin activity assay, 40 µl of test plasma samples were diluted 1:40 and 1:80 in 25 mM Hepes (pH7.5), 150 mM NaCl, and 0.1% BSA (HN/BSA) and incubated in microtiter plate wells with 40 µl of factor Xa/heparin reagent consisting of 3 µg/ml XA (Enzyme Research Lab, IN) and 10 U/ml of unfractionated heparin for 3 min at 37ºC. Subsequently, 40 µl of 1.25 mg/ml chromogenic substrate S-2765 (DiaPharma, OH) was added to each well and the color was analyzed at 405 nm. Standard curves were prepared with each plate by diluting NMP 1:20 to 1:640 in HN/BSA.

Cell isolation and flow cytometry

Single cell suspension from spleen, lymph node, thymus, and bone marrow were subjected to lysis of red blood cells by ammonium chloride. Five hundred thousand cells were labeled in a final volume of 100 µl as described previously (Priatel *et al.*, 2000). Data were acquired using FACScan and analyzed by Cell Quest (Becton Dickinson). All antibodies were obtained from Pharmingen (CA). For PHA lectin flow cytometric analyses of whole blood, 2 µg/ml of FITC-conjugated L-PHA or E-PHA (Vector) was used.

Bone density analysis

Soft tissues were removed and skeletal components were fixed in 10% formalin for 2 days. x-ray images were taken on (Hewlett Packard 43805N Faxitron Series) together with an aluminum alloy reference wedge. The radiograph was scanned on MICROTEK ScanMaker 4, and the density was determined by digital image scanning. Bone density was referenced to results obtained with the aluminum wedge.

Autoantibody titers

Tissue homogenates were coated on 96-well plates and auto-reactivity was quantified using an alkaline phosphatase-congujated anti-mouse Igκ light-chain monoclonal antibody and micro-plate reader at 405 nm as described previously (Chui *et al.*, 2001).

Acknowledgments

We thank our colleagues John Frangos, Jerold Chun, Paul Martin, and Eileen Westerman for helpful comments and additional analyses in the course of these studies. Brad Bendiak graciously provided the *Mgat2* gene sequence for use as probe. This research was funded by grants from the NIH (DK48247 and P01HL57345 to J.D.M. and 1P42 ES 10337–01 to A.W-B.). This work was also supported by the Wellcome Trust and the Biotechnology and Biological Sciences Research Council (to A.D. and H.R.M.). H.S. and J.T. were supported by grants from the Medical Research Council of Canada. J.D.M. is an Investigator of the Howard Hughes Medical Institute.

Abbreviations

ALT, alanine aminotransferase; APPT, activated partial thromboplastin time; AST, aspartate aminotransferase; BSA, bovine serum albumin; CDG, congenital disorder of glycosylation; FAB-MS, fast atom bombardment mass spectrometry; FITC, fluorescein isothiocyanate; GC-MS, gas chromatography mass spectrometry; MS/MS, tandem mass spectrometry; NMP, normal reference mouse plasma; PAS, Periodic acid Schiff; PHA, phytohemagglutinin; TBS, Tris-buffered saline; TRAP, tartrate acid resistant phosphatase activity; vWF, von Willebrand factor.

References

Barlow, C., Hirotsune, S. Paylor, R., Liyanage, M. Eckhaus, M., Collins, F., Shiloh, Y., Crawley, J.N., Ried, T., Tagle, D., and Wynshaw-Boris, A. (1996) *Atm*-deficient mice: a paradigm of ataxia-telangiectasia. *Cell*, **86**, 159–171.

Bennett, M.R. and Florin, T.J. (1974) A statistical analysis of the release of acetylcholine at newly formed synapses in striated muscle. *J. Physiol. (Lond)*, **241**, 515–545.

Carroll, S.M., Hilga, H.H., and Paulson, J.C. (1981) Different cell-surface determinants of antigenically similar influenza virus hemagglutinins. *J. Biol. Chem.*, **256**, 8357–8363.

Charuk, J.H.M., Tan, J., Bernardini, M., Haddad, S., Reithmeier, R.A.F., Jaeken, J., and Schachter, H. (1995) Carbohydrate-deficient glycoprotein syndrome type II: an autosomal recessive N-acetylglucosaminyltransferase II deficiency different from typical hereditary erythroblastic multinuclearity, with a positive acidified-serum lysis test (HEMPAS). *Eur. J. Biochem.*, **230**, 797–805.

Chou, H.H., Takematsu, H., Diaz, S. Iber, J., Nickerson, E., Wright, K.L., Muchmore, E.A., Nelson, D.L., Warren, S.T., and Varki, A. (1998) A mutation in human CMP-sialic acid hydroxylase occurred after the Homo-Pan divergence. *Proc. Natl Acad. Sci. USA*, **95**, 11751–11756.

Chui, D., Oh-Eda, M., Liao, Y. Panneerselvam, K., Lal, A., Marek, K.W., Freeze, H.H., Moreman, K.W., Fukuda, M.N., and Marth, J.D. (1997) Alpha-mannosidase-II deficiency results in dyserythropoiesis and unveils an alternate pathway in oligosaccharide biosynthesis. *Cell*, **90**, 157–167.

Chui, D., Sellakumar, G., Green, R.S., Sutton-Smith, M., McQuistan, T., Marek, K.W., Morris, H.R., Dell, A., and Marth, J.D. (2001) Genetic remodeling of protein glycosylation *in vivo* induces autoimmune disease. *Proc. Natl Acad. Sci. USA*, **98**, 1142–1147.

Cormier-Daire, V., Amiel, J., Vuillaumier-Barrot, S., Tan, J., Durand, G., Munnich, A., Le Merrer, M., and Seta, N. (2000) Congenital disorders of glycosylation IIa cause growth retardation, mental retardation, and facial dysmorphism. *J. Med. Genet.*, **37**, 866–874.

De Lonlay, P., Seta, N., Barrot, S., Chabrol, B., Drouin, V., Gabriel, B.M., Journel, H., Kretz, M., Laurent, J., le Merrer, M., and others. (2001) A broad spectrum of clinical presentations in congenital disorders of glycosylation I: a series of 26 cases. *J. Med. Genet.*, **38**, 14–19.

Demetriou, M., Granovsky, M., Quaggin, S., and Dennis, J.W. (2001) Negative regulation of T-cell activation and autoimmunity by Mgat5 N-glycosylation. *Nature*, **409**, 733–739.

Dupré, T., Barnier, A., de Lonlay, P., Cormier-Daire, V., Durand, G., Codogno, P., and Seta, N. (2000) Defect in N-glycosylation of proteins is tissue-dependent in Congenital Disorders of Glycosylation Ia. *Glycobiology*, **10**, 1277–1281.

Ellgaard, L., Molinari, M., and Helenius, A. (1999) Setting the standards: quality control in the secretory pathway. *Science*, **286**, 1882–1888.

Engelhardt, H., Staudt, M., Hässler, A., Holzbach, U., Freisinger, P., and Krägeloh-Mann, I. (1999) Carbohydrate-deficient glycoprotein syndrome type 2. *J. Inher. Metab.*, **22**, 192–193.

Freeze, H.H. (1998) Disorders in protein glycosylation and potential therapy: tip of an iceberg? *J. Pediatr.*, **133**, 593–600.

Gagneux, P. and Varki, A. (1999) Evolutionary considerations in relating oligosaccharide diversity to biological function. *Glycobiology*, **9**, 747–755.

Galili, U. and Swanson, K. (1991) Gene sequences suggest inactivation of alpha-1, 3-galactosyltransferase in catarrhines after the divergence of apes from monkeys. *Proc. Natl Acad. Sci. USA*, **88**, 7401–7404.

Hogan, B., Beddington, R., Costantini, F., and Lacy, E. (1994) *Manipulating the mouse embryo*. Cold Spring Harbor Laboratory Press, New York.

Hong, S.J. and Chang, C.C. (1989) Use of geographutoxin II (μ-conotoxin) for the study of neuromuscular transmission in the mouse. *Brit. J. Pharmacol.*, **97**, 934–940.

Imtiaz, F., Worthington, V., Champion, M., Beesley, C., Charlwood, J., Clayton, P., Keir, G., Mian, N., and Winchester, B. (2000) Genotypes and phenotypes of patients in the UK with carbohydrate-deficient glycoprotein syndrome type 1. *J. Inherit. Metab. Dis.*, **23**, 162–174.

Ioffe, E. and Stanley, P. (1994) Mice lacking N-acetylglucosaminyltransferase I activity die at mid-gestation, revealing an essential role for complex or hybrid N-linked carbohydrates. *Proc. Natl Acad. Sci. USA*, **91**, 728–732.

Jaeken, J. and Carchon, H. (2000) What's new in congenital disorders of glycosylation? *Eur.. J. Pediatr. Neurol.*, **4**, 163–167.

Jaeken, J., Stibler, H., and Hagberg, B. (1991) The carbohydrate-deficient glycoprotein syndrome: a new multisystemic disease with severe nervous system involvement. *Acta Paediatr. Scand. Suppl.*, **375**, 71.

Jaeken, J., Schachter, H., Carchon, H., de Cock, P., Coddeville, B., and Spik, G. (1994) Carbohydrate deficient glycoprotein syndrome type II: a deficiency in Golgi localised N-acetyl-glucosaminyltransferase II. *Arch. Dis. Child.*, **71**, 123–127.

Jaeken, J., Matthijs, G., Carchon, H., and Van Schaftingen, E. (2001) Defects of N-glycan synthesis. In: Scriver, C.R., Beaudet, A.L., Sly, W.S., and Vallee, D. (eds.), *The metabolic and molecular bases of inherited disease*. McGraw-Hill, New York, pp. 1600–1622.

Katz, B. and Thesleff, S. (1957) On the factors which determine the amplitude of the "miniature endplate potential." *J. Physiol. (Lond)*, **137**, 267–278.

Knopf, C., Rod, R., Jaeken, J., Berant, M., van Schaftingen, E., Fryns, J.P., Brill-Zamir, R., Gershoni-Baruch, R., Lischinsky, S., and Mandel, H. (2000) Transferrin protein variant mimicking carbohydrate-deficient glycoprotein syndrome in trisomy 7 mosaicism. *J. Inherit. Metab. Dis.*, **23**, 399–403.

Koda, Y., Tachida, H., Soejima, M., Takenaka, O., and Kimura, H. (2000) Ancient origin of the null allele se(248) of the human ABO-secretor locus (FUT2). *J. Mol. Evol.*, **50**, 243–248.

Kornfeld, S. (1998) Diseases of abnormal protein glycosylation—an emerging area. *J. Clin. Invest.*, **101**, 1293–1295.

Marquardt, T., Luhn, K., Srikrishna, G., Freeze, H.H., Harms, E., and Vestweber, D. (1999) Correction of leukocyte adhesion deficiency type II with oral fucose. *Blood*, **94**, 3976–3985.

Marth, J.D. (1996) Recent advances in gene mutagenesis by site-directed recombination. *J. Clin. Invest.*, **97**, 1999–2002.

Matthijs, G., Schollen, E., Bjursell, C., Erlandson, A., Freeze, H., Imitiaz, F., Kjaergaard, S., Martinsson, T., Schwartz, M., Seta, N., and others. (2000) Mutations in PMM2 cause congenital disorders of glycosylation, type Ia (CDG-1a). *Hum. Mut.*, **16**, 386–394.

Metzler, M., Gertz, A., Sarkar, M., Schachter, H. Schrader, J.W., and Marth, J.D. (1994) Complex asparagine-linked oligosaccharides are required for morphogenic events during post-implantation development. *EMBO J.*, **13**, 2056–2065.

Mohlke, K.L., Purkayastha, A.A., Westrick, R.J., Smith, P.L., Petryniak, B., Lowe, J.B., and Ginsburg, D. (1999) *Mvwf*, a dominant modifier of murine von Willebrand factor, results from altered lineage-specific expression of a glycosyltransferase. *Cell*, **96**, 111–120.

Niehues, R., Hasilik, M., Alton, G., Korner, C., Schiebe-Sukumar, M., Koch, H.G., Zimmer, K.P., Wu, R., Harms, E., Reiter, K., and others. (1998) Carbohydrate-deficient glycoprotein syndrome type 1b. Phosphomannose isomerase deficiency and mannose therapy. *J. Clin. Invest.*, **101**, 1414–1420.

Parodi, A.J. (2000) Protein glucosylation and its role in protein folding. *Annu. Rev. Biochem.*, **69**, 69–83.

Priatel, J.J., Chui, D., Hiraoka, N., Simmons, C.J.T., Richardson, K.B., Page, D.M., Fukuda, M., Varki, N.M., and Marth, J.D. (2000) The ST3Gal-I sialyltransferase controls $CD8^+$ T cell homeostasis by modulating O-glycan biosynthesis. *Immunity*, **12**, 273–283.

Russell, L.D., Ettlin, R.A., Hikim, A.P.S., and Clegg, E.D. (1990) Staging for laboratory species. In: *Histological and histopathological evaluation of the testis*. Cache River Press, Clearwater, FL, pp. 62–194.

Schachter, H. (1991). The "yellow brick road" to branched complex N-glycans. *Glycobiology*, **1**, 453–461.

Schachter, H. and Jaeken, J. (1999) Carbohydrate-deficient glycoprotein syndrome type II. *Biochim. Biophys. Acta*, **1455**, 179–192.

Schofield, G.G. and Marshall, I.G. (1980) Neuromuscular transmission in the athymic nude mouse. *J. Neurolog. Sci.*, **48**, 21–34.

Shafi, R., Iyer, S.P.N., Ellies, L.G., O'Donnell, N., Marek, K.W., Chui, D., Hart, G.W., and Marth, J.D. (2000) The O-GlcNAc transferase gene resides on the X chromosome and is essential for embryonic stem cell viability and mouse ontogeny. *Proc. Natl Acad. Sci. USA*, **97**, 5735–5739.

Sutton-Smith, M., Morris, H.R., and Dell, A. (2000) A rapid mass spectrometric strategy suitable for the investigation of glycan alterations in knockout mice. *Tetrahedron Asymmetry*, **11**, 363–369.

Suzuki, Y., Ito, T., Suzuki, T., Holland, R.E. Jr., Chambers, T.M., Kiso, M., Ishida, H., and Kawaoka, Y. (2000) Sialic acid species as a determinant of the host range of influenza A viruses. *J. Virol.*, **74**, 11825–11831.

Tan, J., Dunn, J., Jaeken, J., and Schachter, H. (1996) Mutations in the *MGAT2* gene controlling complex N-glycan synthesis cause carbohydrate-deficient glycoprotein syndrome type II, an autosomal recessive disease with defective brain development. *Am. J. Hum. Genet.*, **59**, 810–817.

Teng-umnuay P., Morris, H.R., Dell A., Panico M., Paxton T., and West C.M. (1998) The cytoplasmic F-box binding protein SKP1 contains a novel pentasaccharide linked to hydroxyproline in *Dictyostelium*. *J. Biol. Chem.*, **273**, 18242–18249.

Wada, Y. Nikishawa, A., Okamoto, N., Inui, K., Tsukamoto, H., Okada, S., and Taniguchi, N. (1992) Structure of serum transferrin in carbohydrate-deficient glycoprotein syndrome. *Biochem. Biophys. Res. Commun.*, **189**, 832–836.

Westphal, V., Srikrishna, G., and Freeze, H.H. (2000) Congenital disorders of glycosylation: have you encountered them? *Genet. Med.*, **2**, 329–337.

Yamashita, K., Hiroko, I., Ohkura, T., Fukushima, K., Yuasa, I., Ohno, K., and Takeshita, K. (1993) Sugar chains of serum transferrin from patients with carbohydrate deficient glycoprotein syndrome. *J. Biol. Chem.*, **268**, 5783–5789.